Supporting Information

Discovery of a Fungal Copper Radical Oxidase with High Catalytic Efficiency Towards 5-hydroxymethylfurfural and Benzyl Alcohols for Bioprocessing.

Yann Mathieu[1], Wendy A. Offen[2], Stephanie M. Forget[1,3], Luisa Ciano[3,+], Alexander Holm Viborg[1], Elena Blagova[3], Bernard Henrissat[4,5], Paul H. Walton[3], Gideon J. Davies[3], Harry Brumer[1.2.6.7,]∗

[1]Michael Smith Laboratories, University of British Columbia, 2185 East Mall, Vancouver, BC, V6T 1Z4, Canada;

[2]Department of Chemistry, University of York, Heslington, YO10 5DD, York, UK.

[3]Department of Chemistry, University of British Columbia, 2036 Main Mall, Vancouver, BC, V6T 1Z1, Canada;

[4]Architecture et Fonction des Macromolécules Biologiques (AFMB), CNRS, Aix-Marseille University, Marseille, 13288, France;

[5]INRA, USC1408 Architecture et Fonction des Macromolécules Biologiques (AFMB), Marseille, 13288, France;

[6]Department of Biochemistry and Molecular Biology, University of British Columbia, 2350 Health Sciences Mall, Vancouver, BC, V6T 1Z3, Canada;

[7]Department of Botany, University of British Columbia, 3200 University Boulevard, Vancouver, BC, V6T 1Z4, Canada

[+] Current address: School of Chemistry and Photon Science Institute, University of Manchester, Oxford Road, Manchester, M13 9PL, UK

Corresponding Author

*Harry Brumer: brumer@msl.ubc.ca

Supporting Tables

Table S1: Initial activity screens* of *Cgr*AAO-WT and its variants

	Substrate	Specific activity (µmole.min^{-1}.mg^{-1})		
		***Cgr*AAO-WT**	**CgrAAO-Y334F**	***Cgr*AAO-Y334W**
Carbohydrates	D-Galactose (300 mM)	1.80 ± 0.03	4.1 ± 0.1	34.9 ± 0.3
	D-Lactose (300 mM)	1.93 ± 0.05	4.4 ± 0.1	12.6 ± 0.3
	Melibiose (300 mM)	9.9 ± 0.7	20.6 ± 1.2	46.9 ± 0.5
	Raffinose (300 mM)	8.5 ± 0.1	38.3 ± 1.1	51.4 ± 0.3
	D-Glucose (300 mM)	0.050 ± 0.002	n.m.§	n.m.§§
	D-Xylose (300 mM)	0.950 ± 0.005	3.80 ± 0.08	0.88 ± 0.01
	L-Arabinose (300 mM)	0.74 ± 0.01	n.m.§	n.m.§
	D-Ribose (300 mM)	0.37 ± 0.01	0.67 ± 0.01	0.38 ± 0.03
	D-Fructose (300 mM)	0.117 ± 0.006	n.m.§	n.m.§
	D-Mannose	0.066 ± 0.004	n.m.§	0.070 ± 0.006
	Sucrose (300 mM)	0.045 ± 0.001	n.m.§	n.m.§
	Maltose (300 mM)	0.051 ± 0.002	n.m.§	n.m.§
	Cellobiose (300 mM)	0.115 ± 0.002	n.m.§	0.14 ± 0.01
	Carob Galactomannan (2.5 mg.mL^{-1})	0.43 ± 0.02	0.90 ± 0.02	0.063 ± 0.004
	Xyloglucan (2.5 mg.mL-1)	0.060 ± 0.002	n.m.§	n.m.§
Polyols	Glycerol (300 mM)	7.2 ± 0.4	18.4 ± 0.3	12.3 ± 0.4
	Sorbitol (300 mM)	0.760 ± 0.007	0.60 ± 0.03	0.32 ± 0.02
Diols	1,2-Propanediol (300 mM)	4.02 ± 0.04	6.3 ± 0.2	0.35 ± 0.02
	1,3-Propanediol (300 mM)	10.9 ± 0.1	42.7 ± 0.9	1.87 ± 0.03
	1,4-Butanediol (300 mM)	2.6 ± 0.1	n.m.§	2.2 ± 0.1
Aldehyde	Methyl glyoxal (5 mM)	n.m.§	1.3 ± 0.1	n.m.§
Primary Alcohols	Methanol (300 mM)	0.81 ± 0.02	1.50 ± 0.07	0.19 ± 0.01
	Ethanol (300 mM)	0.42 ± 0.04	0.70 ± 0.01	0.050 ± 0.002
	1-Butanol (300 mM)	0.85 ± 0.02	n.m.§	n.m.§
	1-Propanol (300 mM)	0.50 ± 0.01	n.m.§	n.m.§
Secondary Alcohols	2-Propanol (10 mM)	0.036 ± 0.002	n.m.§	n.m.§
	1-Phenyl Ethanol (10 mM)	n.m.§	n.m.§	n.m.§
	2-Phenyl Ethanol (10 mM)	n.m.§	n.m.§	n.m.§
Benzyl Alcohols	Benzyl alcohol (5 mM)	3.4 ± 0.1	10.6 ± 0.1	1.24 ± 0.06
	m-Anisyl alcohol (5 mM)	3.1 ± 0.2	8.2 ± 0.2	1.63 ± 0.05
	p-Anisyl alcohol (5 mM)	2.9 ± 0.1	6.6 ± 0.2	1.03 ± 0.02
	Veratryl alcohol (5 mM)	3.71 ± 0.05	10.8 ± 0.3	1.48 ± 0.08
	Cinnamyl alcohol (5 mM)	2.8 ± 0.2	6.4 ± 0.3	0.64 ± 0.08
	4-Hydroxy benzyl alcohol (5 mM)	3.3 ± 0.1	7.8 ± 0.4	1.3 ± 0.1
	Coniferyl alcohol (5 mM)	n.m.§	n.m.§	n.m.§
Furans	HMF (5 mM)	26.4 ± 1.1	16.4 ± 0.9	1.39 ± 0.06
	HMFCA (5 mM)	2.8 ± 0.3	2.1 ± 0.1	0.66 ± 0.04
	DFF (5 mM)	0.0010 ± 0.0001	0.051 ± 0.001	0.100 ± 0.005
	FFCA (5 mM)	0.0020 ± 0.0001	0.003 ± 0.001	0.0030 ± 0.0001

* Measurements were performed in triplicates at 25 °C in 100 mM sodium phosphate buffer pH 7 using the HRP/ABTS assay. Activities were monitored using concentrations indicated within parentheses for each substrate.

§No activity detected with a specific activity limit of detection of 9 x 10^{-4} µmole.min^{-1}.mg^{-1} using 65 µmole of protein, which is 5-fold

Table S2: EPR spin Hamiltonian parameters from simulations of cw X band spectra for *Cgr*AAO-WT, -Y334F and –Y334W[a]

		***Cgr*AAO-WT**	***Cgr*AAO-Y334F**	***Cgr*AAO-Y334W**
	g_1	2.059	2.059	2.049
***g* values**	g_2	2.072	2.072	2.061
	g_3	2.278	2.278	2.275
	$\|A_1\|$	40	40	50
A_{Cu} (MHz)	$\|A_2\|$	45	40	50
	$\|A_3\|$	530	530	515
SHF A_N principal values (MHz) *		43, 43	43, 43	45, 45
		±3	±3	±3
A_{cu} strains (MHz)		55, 65, 130	35, 75, 130	50, 65, 130
Line widths (mT)		0.7, 0.7	0.7, 0.7	0.8, 0.8
Frequency (GHz)		9.2986	9.2995	9.2982

* error estimated from quality of simulated fits

[a]. Spectra were recorded in the presence of 10% glycerol in 100 mM Na phosphate buffer pH 7.0. For coupled nitrogen nuclei, only the principal coupling value could be determined from the simulations of the superhyperfine (SHF); the two values refer to the two different N nuclei.

Table S3: Comparison of catalytic parameters of *Cgr*AAO with other enzymes acting on HMF and its derivatives*

	HMF			DFF			HMFCA			FFCA		
	K_m (mM)	k_{cat} (s^{-1})	k_{cat}/K_m ($M^{-1}.s^{-1}$)	K_m (mM)	k_{cat} (s^{-1})	k_{cat}/K_m ($M^{-1}.s^{-1}$)	K_m (mM)	k_{cat} (s^{-1})	k_{cat}/K_m ($M^{-1}.s^{-1}$)	K_m (mM)	k_{cat} (s^{-1})	k_{cat}/K_m ($M^{-1}.s^{-1}$)
Bacterial HMFO[a]	1.4	9.9	7.1×10^3	1.7	1.6	940	73	8.5	120	NM	NM	<10
***Per*AAO**[b]	1.6 ± 0.2	0.33 ± 0.01	220 ± 43	3.3 ± 0.2	0.52 ± 0.01	158.0 ± 9.2	NM	NM	NM	NM	NM	NM
MtGLOx[c]	20.2 ± 9.0	15.9	982	NM	NM	NM	NA	NA	NA	NA	NA	NA
Pciglox1[d]	15.66 ± 2.35	1.59 ± 0.12	101.66 ± 0.01	4.38 ± 0.1	0.54 ± 0.24	124.39 ± 0.01	NA	NA	NA	0.85 ± 0.14	0.03 ± 0.01	38.55 ± 0.01
Pciglox2[d]	5.87 ± 2.04	0.56 ± 0.09	96.04 ± 0.01	0.21 ± 0.04	4.80 ± 0.24	$2.34 \pm 0.01 \times 10^4$	NA	NA	NA	1.40 ± 0.39	2.02 ± 0.03	$1.40 \pm 0.01 \times 10^3$
Pciglox3[d]	6.35 ± 1.32	0.75 ± 0.07	118.35 ± 0.01	0.18 ± 0.05	1.28 ± 0.09	$7.30 \pm 0.01 \times 10^3$	NA	NA	NA	0.61 ± 0.58	0.04 ± 0.01	72.03 ± 0.01
***Cgr*AAO**[e]	6.5 ± 0.3	126.0 ± 1.5	$1.94 \pm 0.09 \times 10^4$	NM	NM	NM	26.9 ± 3.0	28.3 ± 1.3	$1.1 \pm 0.1 \times 10^3$	NM	NM	NM

* NM not measurable; NA non assessed

[a] Kinetic data from [1]; [b] Kinetic data from [2]; [c] Kinetic data from [3]; [d] Kinetic data from [4]; [e] Kinetic data derive from Table 1

Table S4 : PCR primers[a]

	Primers name	Primers sequence 5' - 3'
Mutagenesis	*Cgr*AAO-Y334W-f	GGTGGGCTTggTCAGGTGAGC
	*Cgr*AAO-Y334W-r	AATAGTGAAGACCTTACCATTAC
	*Cgr*AAO-Y334F-f	GGTGGGGCTTtTTCAGGTGAG
	*Cgr*AAO-Y334F-r	AATAGTGAAGACCTTACCATTAC

[a]. Primer sequences used for site directed mutagenesis. Mutated bases are in lowercase.

Supporting Figures

A

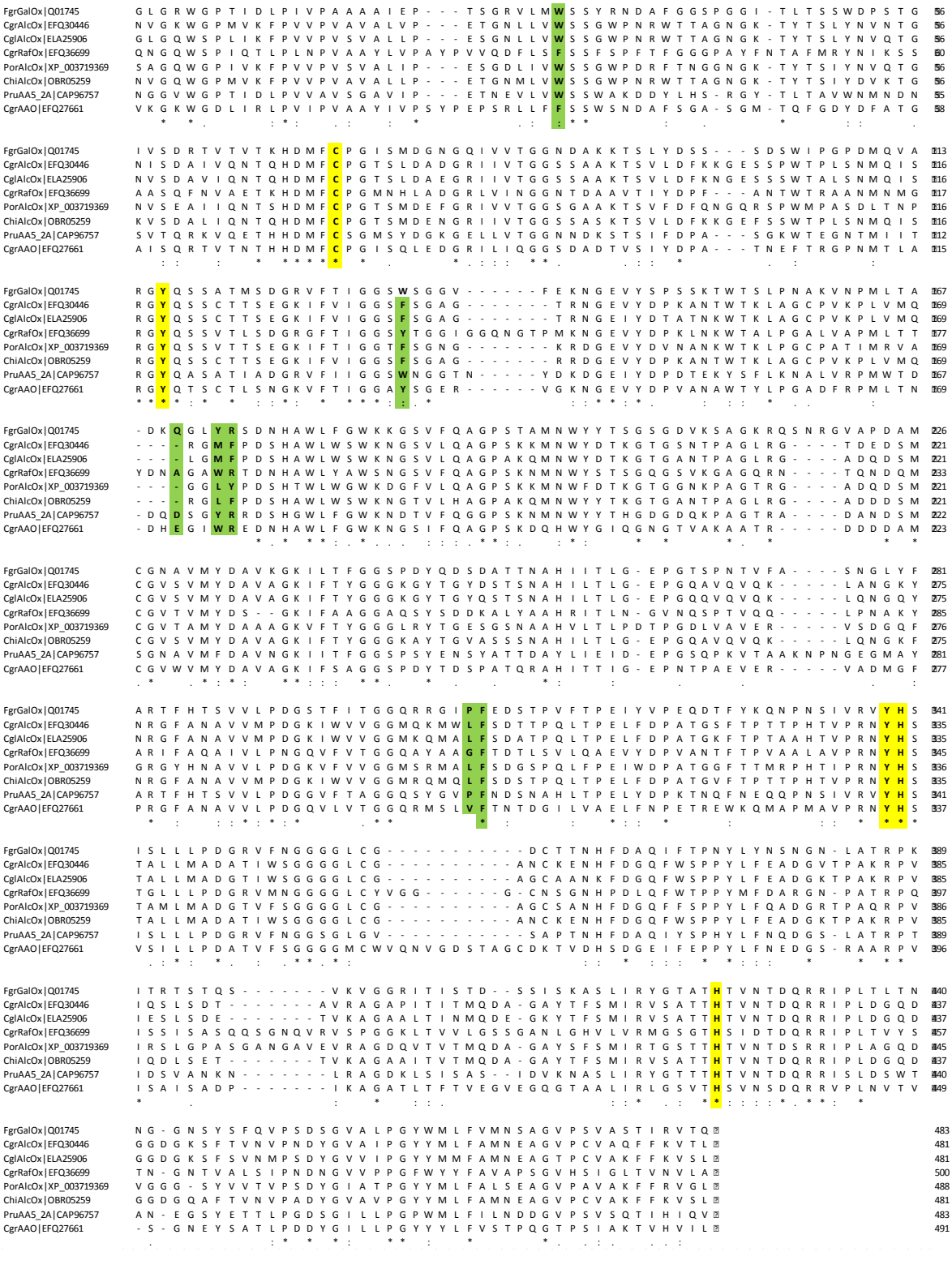

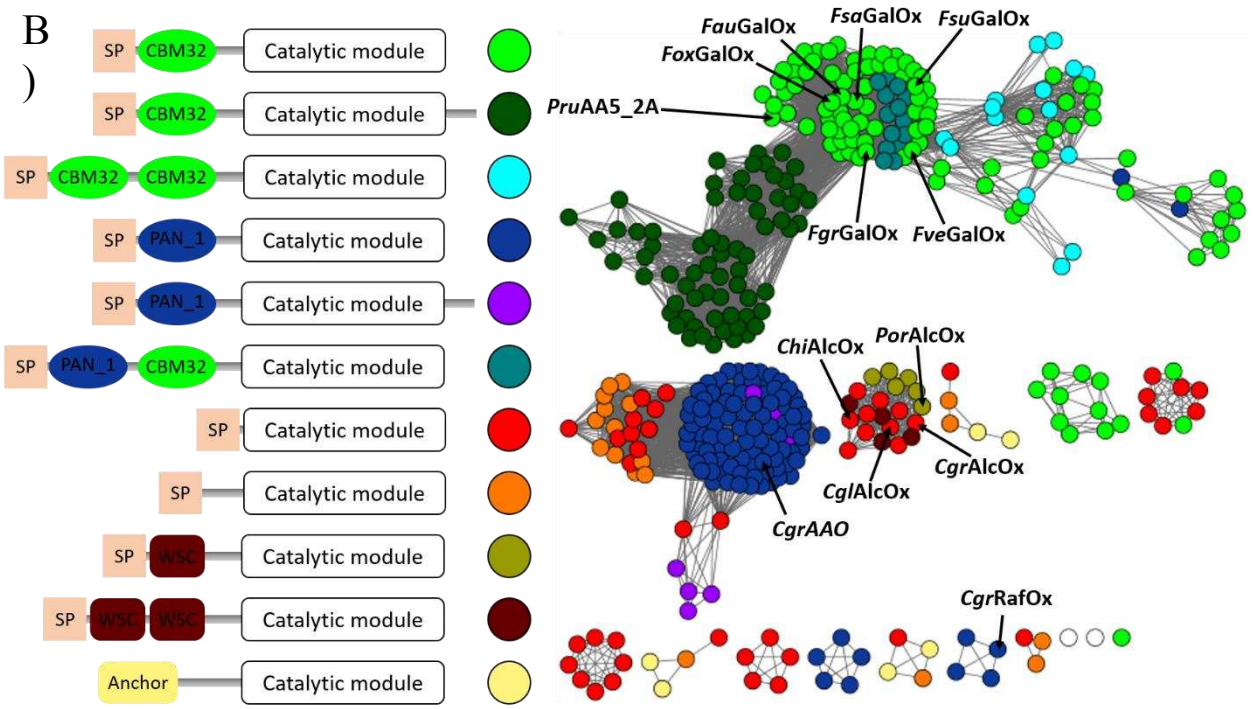

Figure S1. (A) Sequence alignment of *Colletotrichum graminicola* aryl alcohol oxidase (*Cgr*AAO) with characterized AA5_2 members. (B) Sequence similarity network at an alignment score cut-off of 10^{-550} of 392 catalytic modules from the AA5_2 subfamily with their corresponding modularity. For each panel, predicted native signal peptides and additional N-terminal modules have been removed. Conserved active-site catalytic residues and residues involved in substrate recognition are highlighted in yellow and green, respectively (A). Each node is colored according to its modularity. Catalytic modules are shown in white, carbohydrate binding modules are in green [5], PAN_1 domains are blue [6], WSC are brown [7] and GPI anchor are yellow (B). *Cgr*AlcOx = *Colletotrichum graminicola* alcohol oxidase, *Cgl*AlcOx = *Colletotrichum gloeosporioides* alcohol oxidase, *Cgr*RafOx = *Colletotrichum graminicola* raffinose oxidase, *Pru*AA5_2A = *Penicillium rubens Wisconsin 54–1255* AA5_2 oxidase, *Fgr*GalOx = *Fusarium graminearum* galactose oxidase, *Chi*AlcOx = *Colletotrichum higginsianum* alcohol oxidase and *Por*AlcOx = *Pyricularia oryzae* alcohol oxidase.

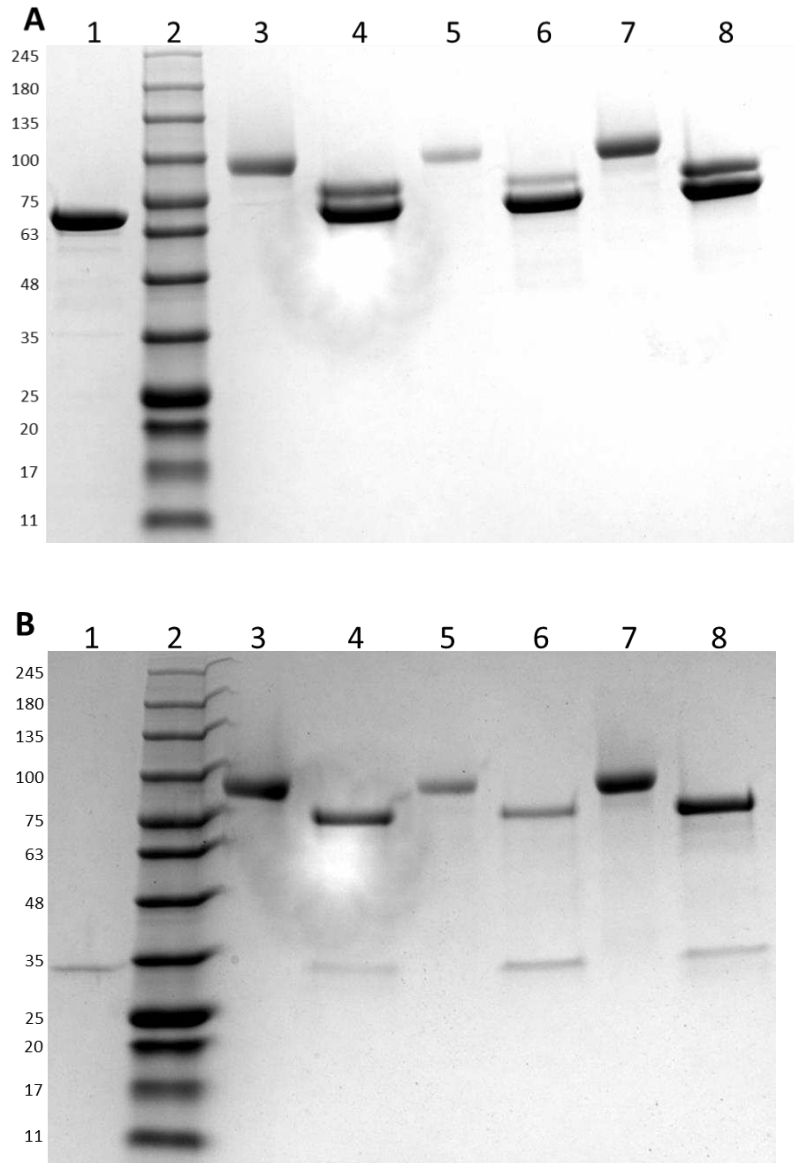

Figure S2. SDS-PAGE of *Cgr*AAO-WT, *Cgr*AAO-Y334F and *Cgr*AAO-Y334W & *N*-deglycosylation studies.

Enzymes were *N*-deglycosylated under denaturing conditions with either PNGaseF (A) or EndoH (B).

(A): 1: EndoH, 2: molecular weight marker, 3: *Cgr*AAO-WT (5 µg), 4: *Cgr*AAO-WT (5 µg) + EndoH, 5: *Cgr*AAO-Y334W (5 µg), 6: *Cgr*AAO-Y334W (5 µg) + EndoH, 7: *Cgr*AAO-Y334F (5 µg), 8: *Cgr*AAO-Y334F (5 µg) + EndoH

(B): 1: PNGaseF, 2: molecular weight marker, 3: *Cgr*AAO-WT (5 µg), 4: *Cgr*AAO-WT (5 µg) + PNGaseF, 5: *Cgr*AAO-Y334W (5 µg), 6: *Cgr*AAO-Y334W (5 µg) + PNGaseF, 7: *Cgr*AAO-Y334F (5 µg), 8: *Cgr*AAO-Y334F (5 µg) + PNGaseF

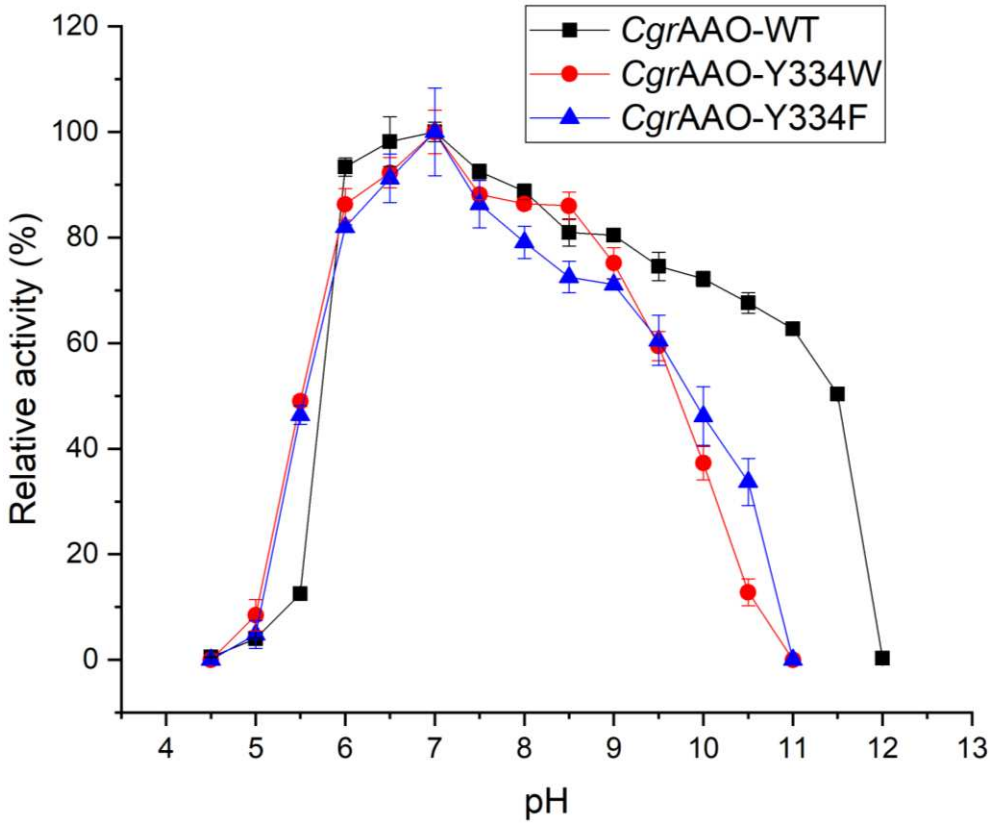

Figure S3. pH-rate profiles of *Cgr*AAO-WT and mutants. Data are represented as means ± standard deviations (n = 3). Activities were determined by the HRP/ABTS assay monitoring absorbance at 420 nm using 50 mM HMF for *Cgr*AAO-WT and *Cgr*AAO-Y334F, and 500 mM melibiose for *Cgr*AAO-Y334W. pH rate profiles were determined after 1-min incubations at the desired pH, pH range 4-6 was maintained using 100 mM phosphate-citrate buffers, pH range 6-8 was maintained using 100 mM phosphate buffers and pH range 8- 12 was maintained using glycine-sodium hydroxide buffers.

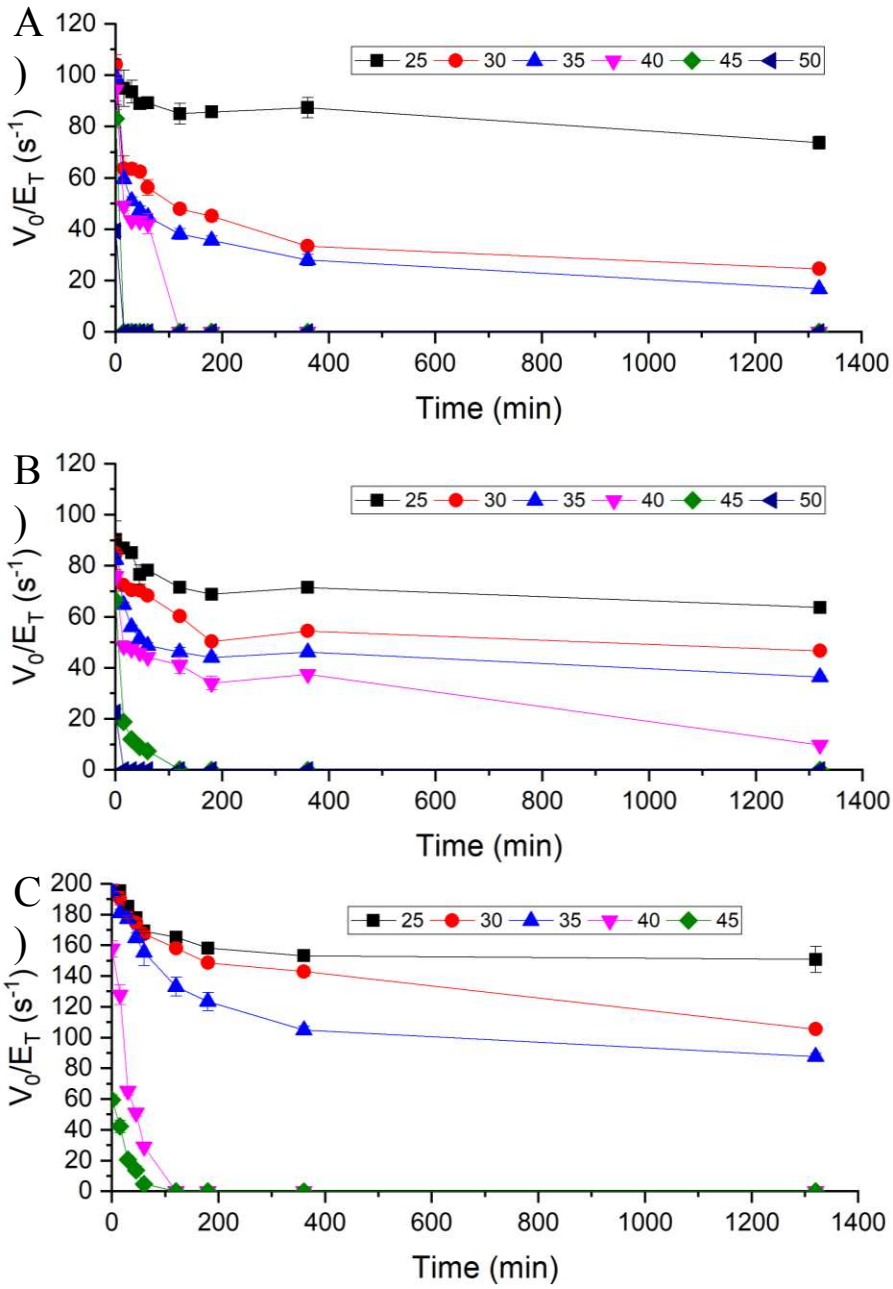

Figure S4. Temperature stability. A) *Cgr*AAO-WT; B) *Cgr*AAO-Y334W; C) *Cgr*AAO-Y334F. Data are represented as means ± standard deviations (n = 3). Activities values were determined by the coupled HRP/ABTS at each temperature, maintained by a gradient thermocycler, using 50 mM HMF for *Cgr*AAO-WT and *Cgr*AAO-Y334F, and 500 mM melibiose for *Cgr*AAO-Y334W.

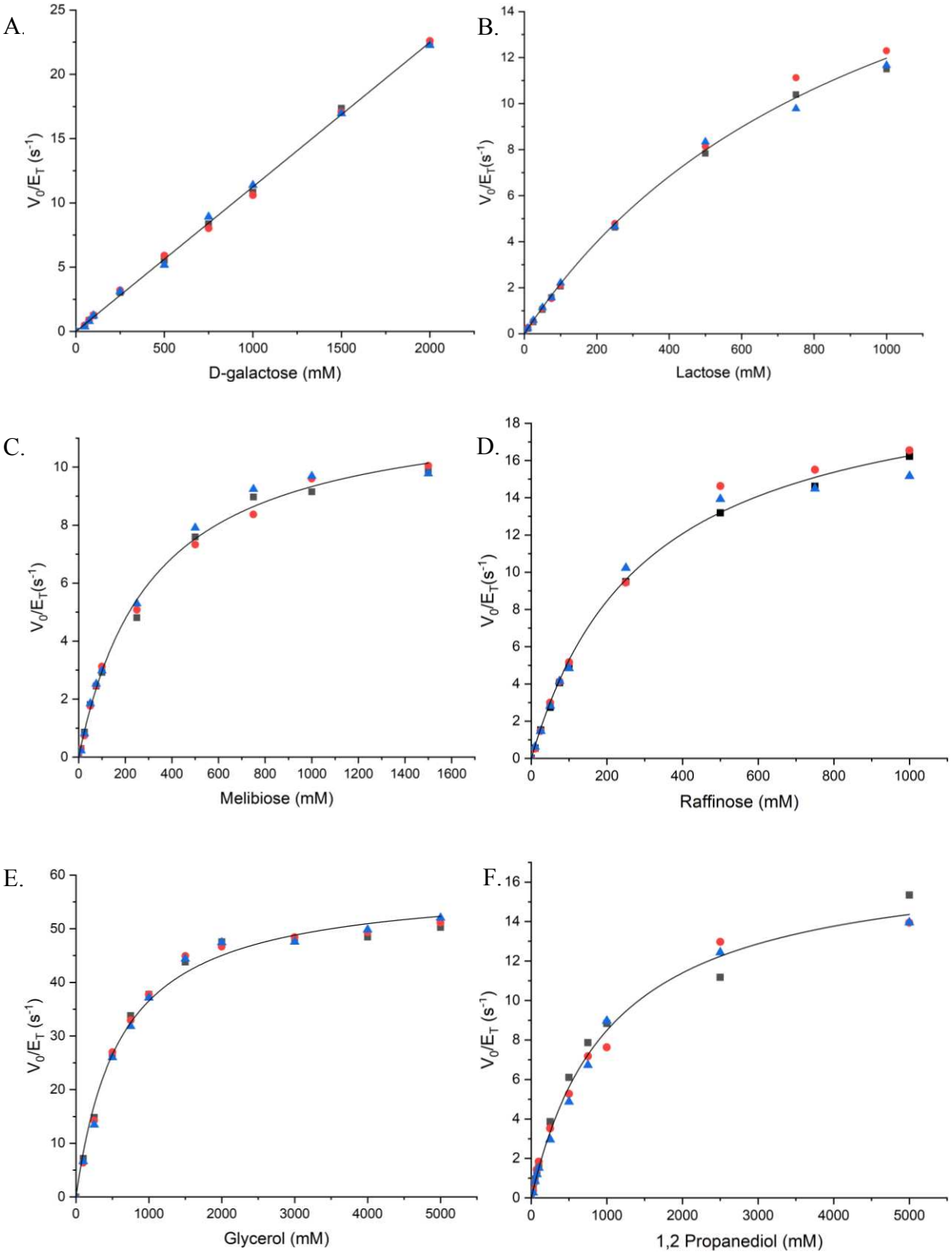
A.
V_0/E_T (s^{-1})
D-galactose (mM)
B.
V_0/E_T(s^{-1})
Lactose (mM)
C.
V_0/E_T(s^{-1})
Melibiose (mM)
D.
V_0/E_T(s^{-1})
Raffinose (mM)
E.
V_0/E_T (s^{-1})
Glycerol (mM)
F.
V_0/E_T (s^{-1})
1,2 Propanediol (mM)

G.

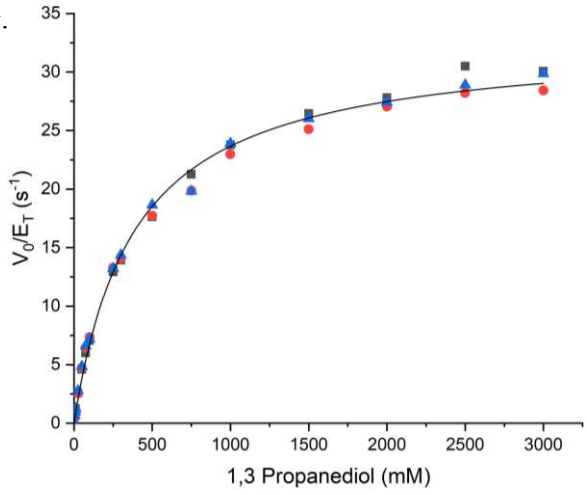
V_0/E_T (s^{-1})
1,3 Propanediol (mM)

H.

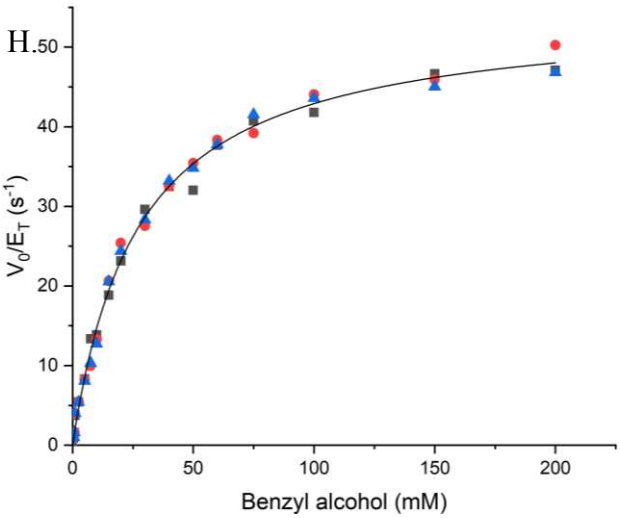
V_0/E_T (s^{-1})
Benzyl alcohol (mM)

I.

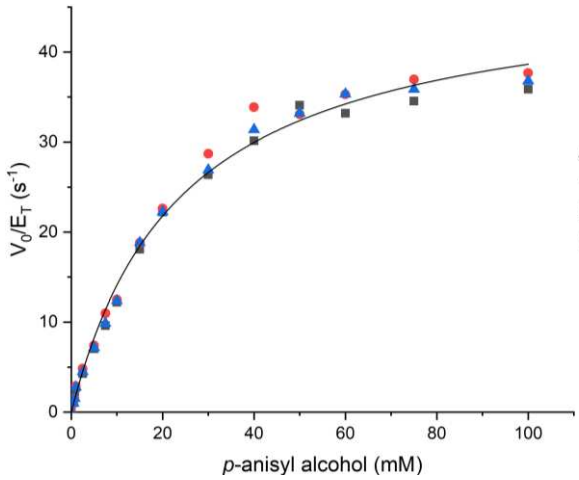
V_0/E_T (s^{-1})
p-anisyl alcohol (mM)

J.

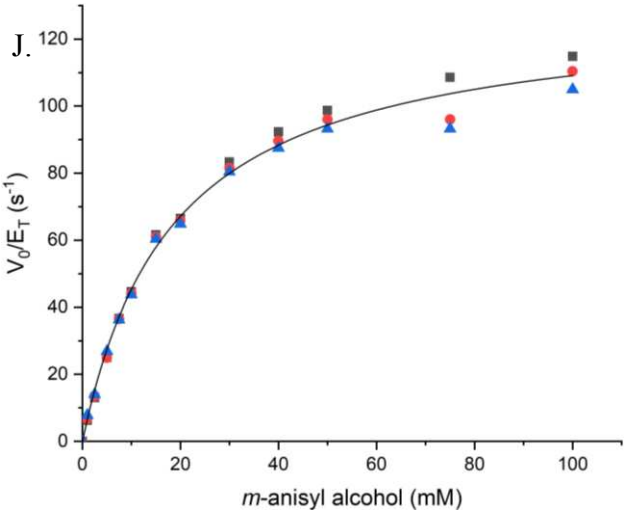
V_0/E_T (s^{-1})
m-anisyl alcohol (mM)

K.

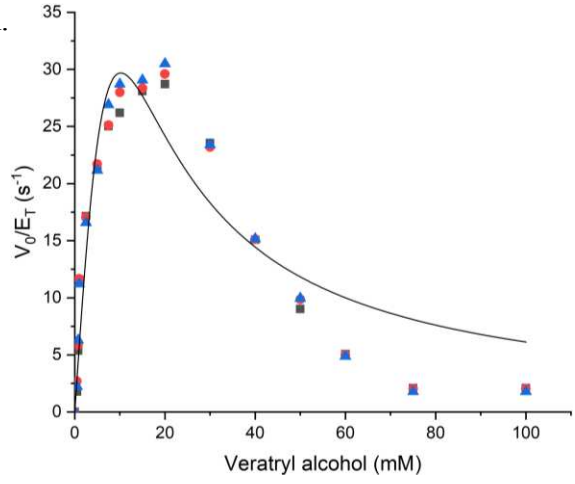
V_0/E_T (s^{-1})
Veratryl alcohol (mM)

L.

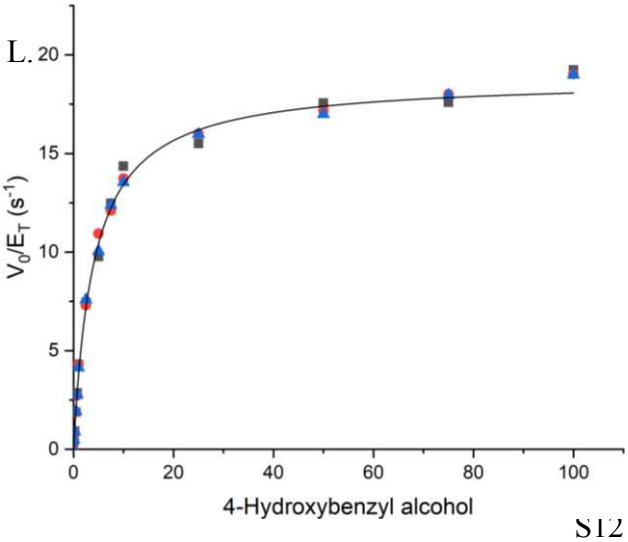
V_0/E_T (s^{-1})
4-Hydroxybenzyl alcohol

M.

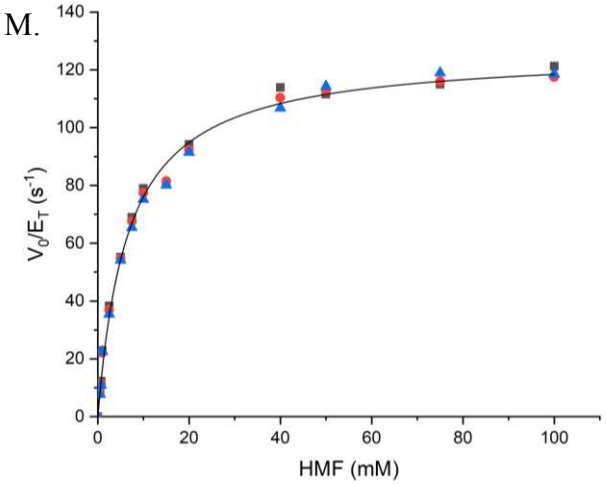
V_0/E_T (s^{-1})
HMF (mM)

N.

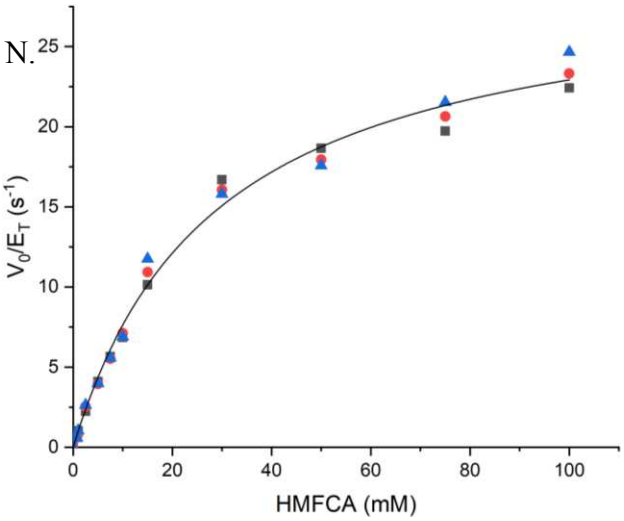
V_0/E_T (s^{-1})
HMFCA (mM)

A’

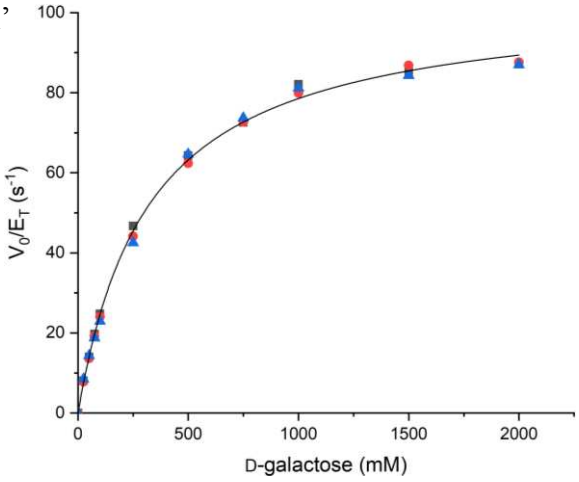
V_0/E_T (s^{-1})
D-galactose (mM)

B’.

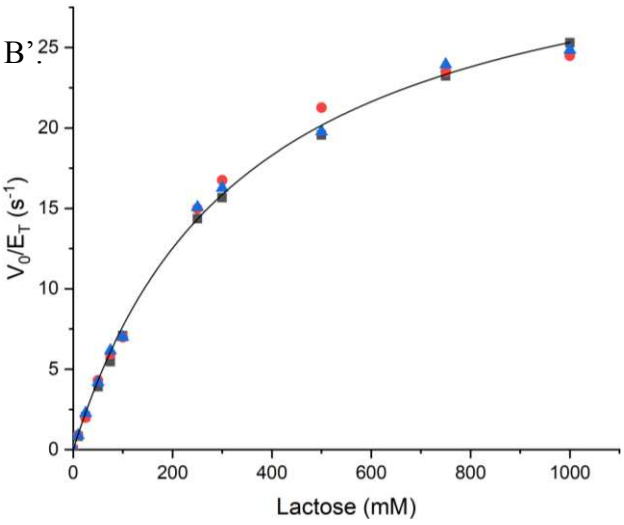
V_0/E_T (s^{-1})
Lactose (mM)

C’.

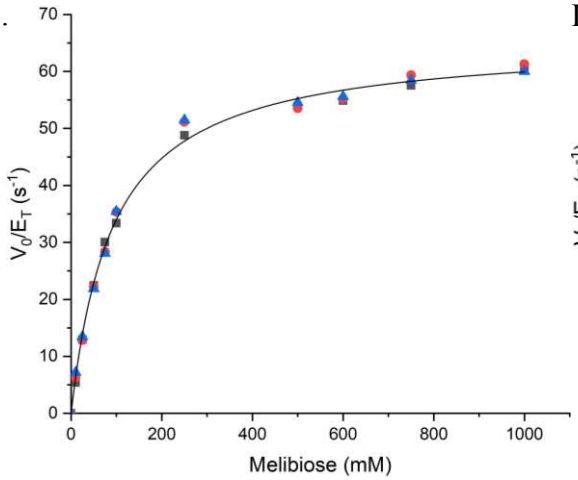
V_0/E_T (s^{-1})
Melibiose (mM)

D’

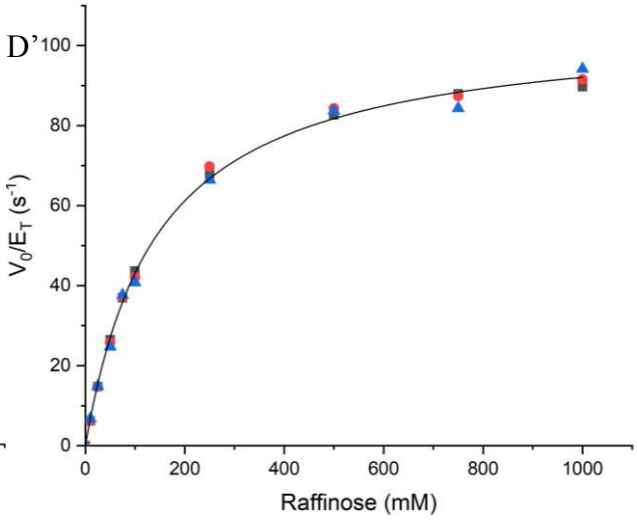
V_0/E_T (s^{-1})
Raffinose (mM)

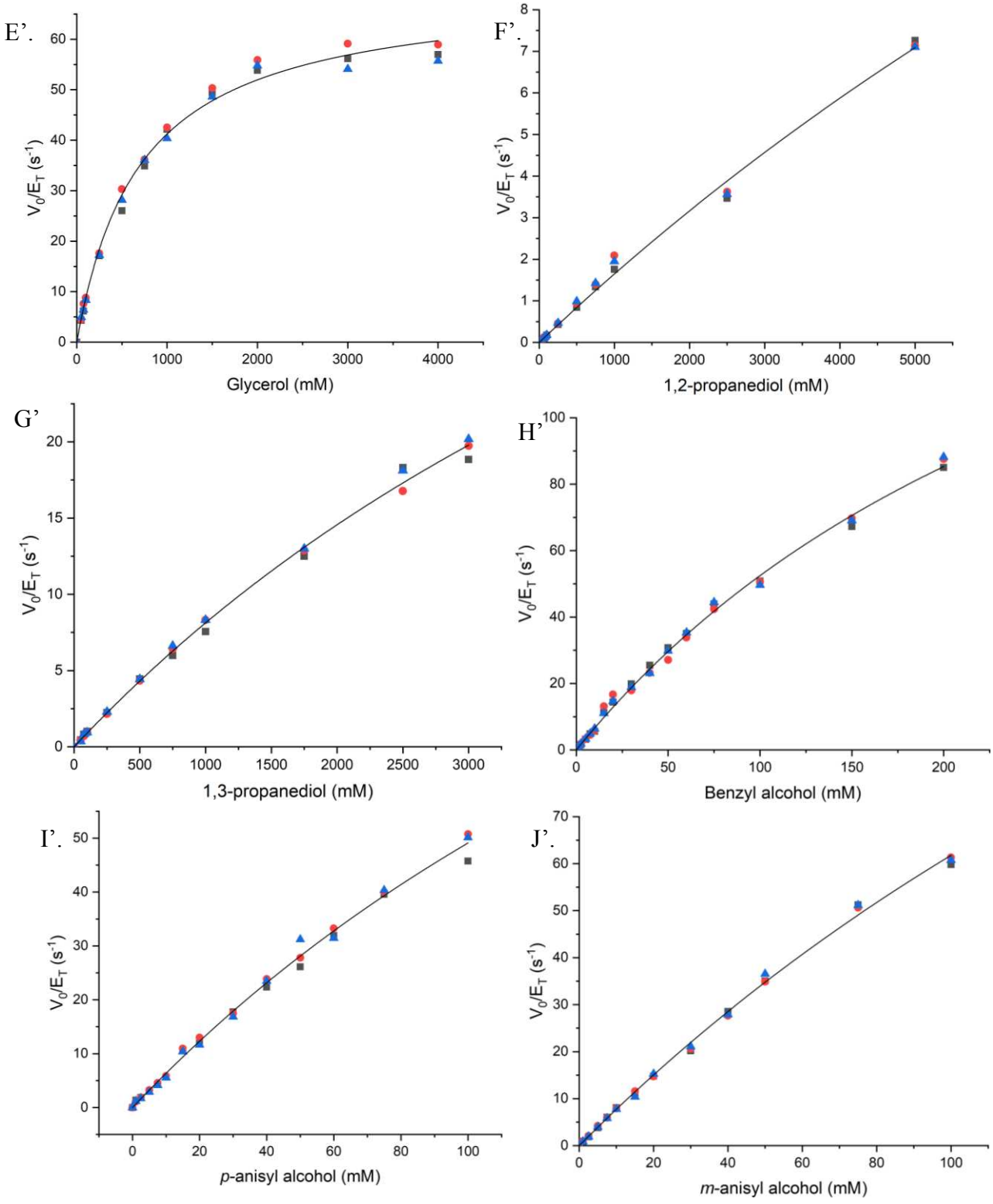
E'.
F'.
G'
H'
I'.
J'.
V_0/E_T (s^{-1})
Glycerol (mM)
1,2-propanediol (mM)
1,3-propanediol (mM)
Benzyl alcohol (mM)
p-anisyl alcohol (mM)
m-anisyl alcohol (mM)

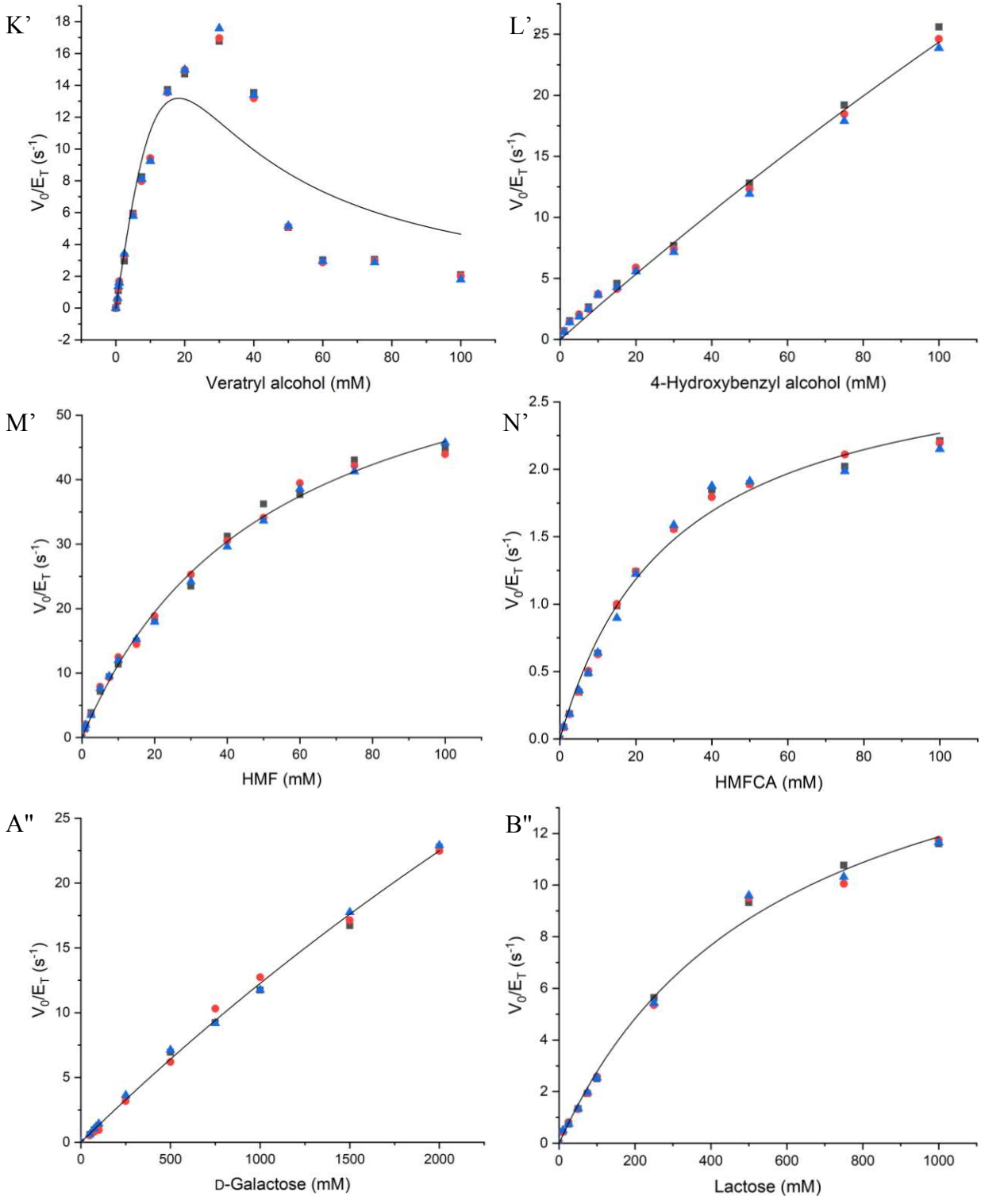
K'
V_0/E_T (s^{-1})
Veratryl alcohol (mM)
L'
V_0/E_T (s^{-1})
4-Hydroxybenzyl alcohol (mM)
M'
V_0/E_T (s^{-1})
HMF (mM)
N'
V_0/E_T (s^{-1})
HMFCA (mM)
A"
V_0/E_T (s^{-1})
D-Galactose (mM)
B"
V_0/E_T (s^{-1})
Lactose (mM)

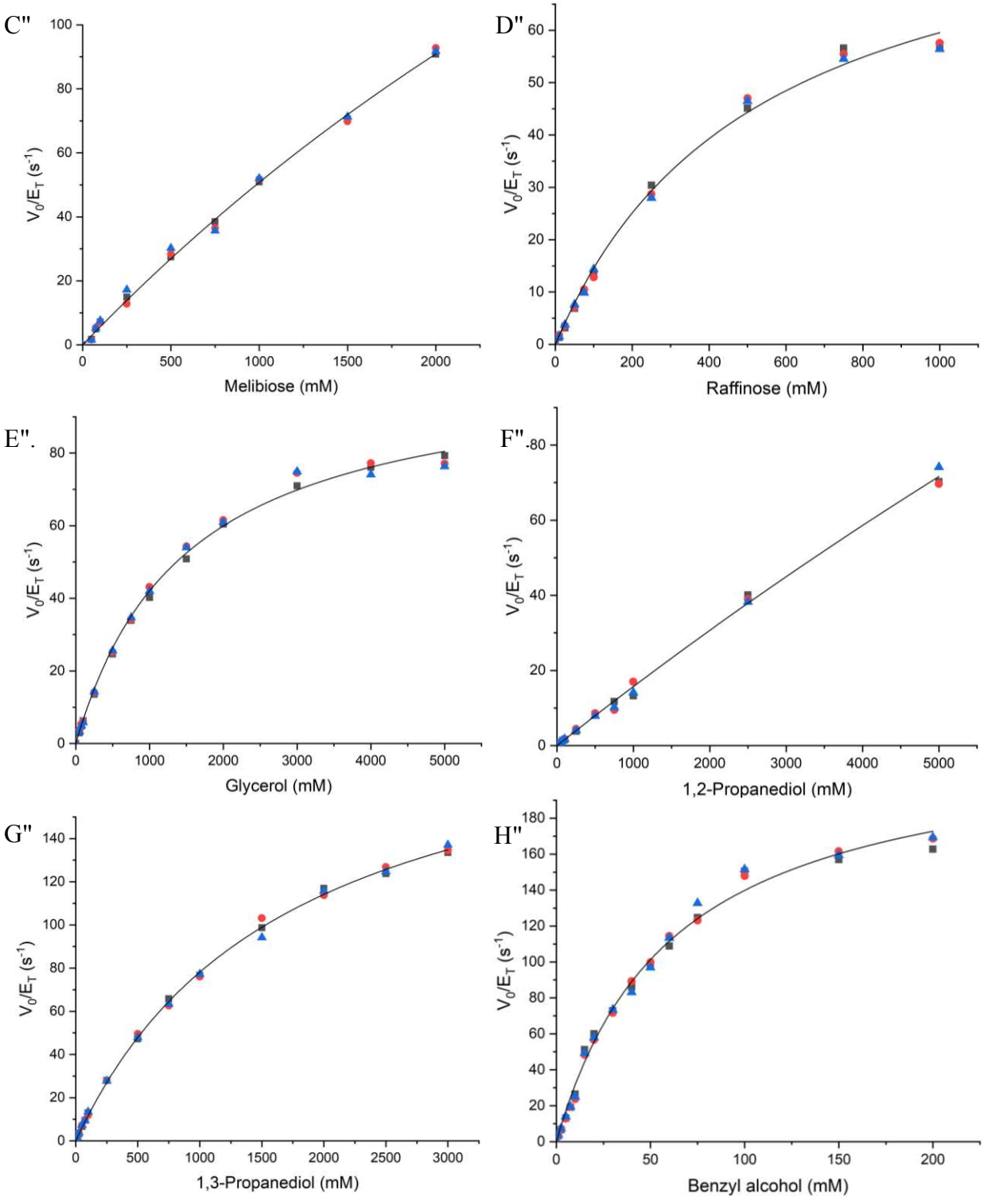
C"
V_0/E_T (s^{-1})
Melibiose (mM)
D"
V_0/E_T (s^{-1})
Raffinose (mM)
E".
V_0/E_T (s^{-1})
Glycerol (mM)
F"
V_0/E_T (s^{-1})
1,2-Propanediol (mM)
G"
V_0/E_T (s^{-1})
1,3-Propanediol (mM)
H"
V_0/E_T (s^{-1})
Benzyl alcohol (mM)

I".

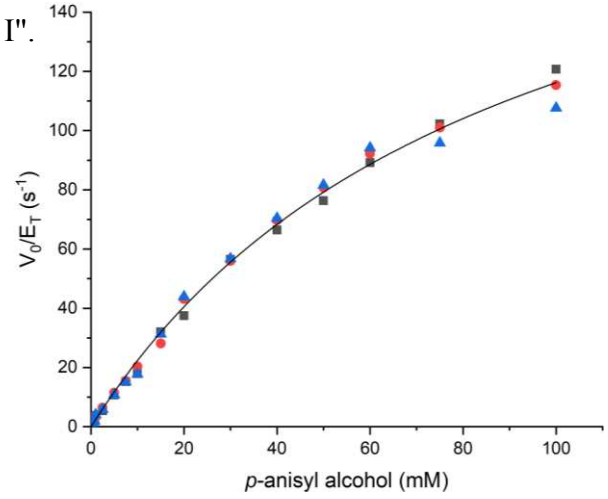
V_0/E_T (s^{-1})
p-anisyl alcohol (mM)

J".

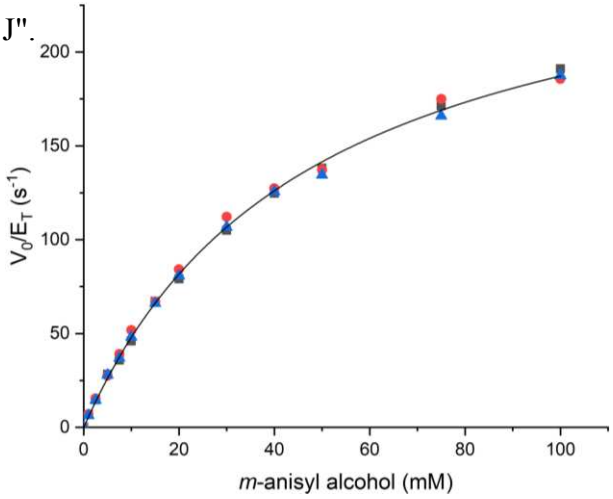
V_0/E_T (s^{-1})
m-anisyl alcohol (mM)

K"

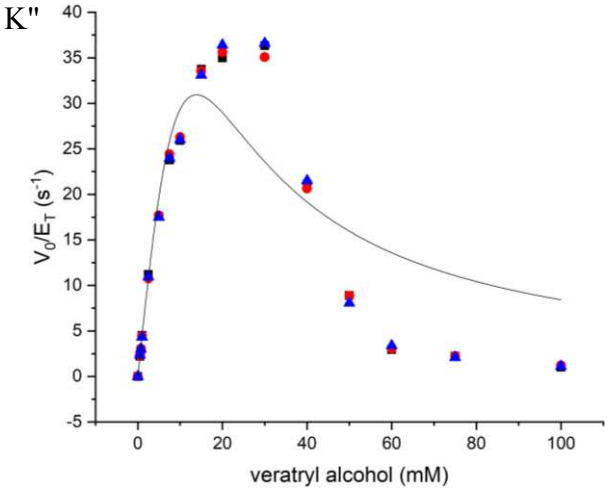
V_0/E_T (s^{-1})
veratryl alcohol (mM)

L".

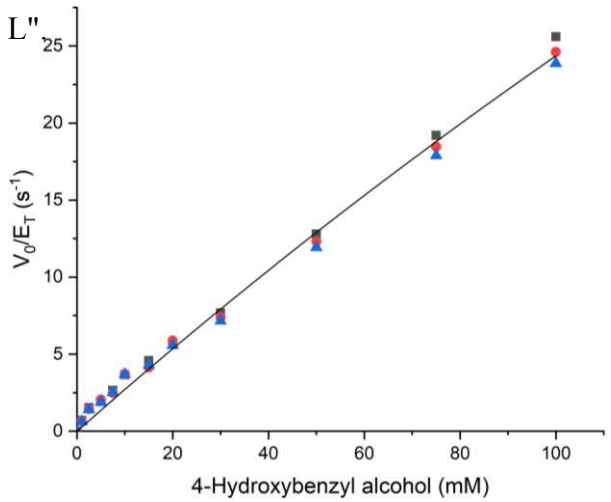
V_0/E_T (s^{-1})
4-Hydroxybenzyl alcohol (mM)

M

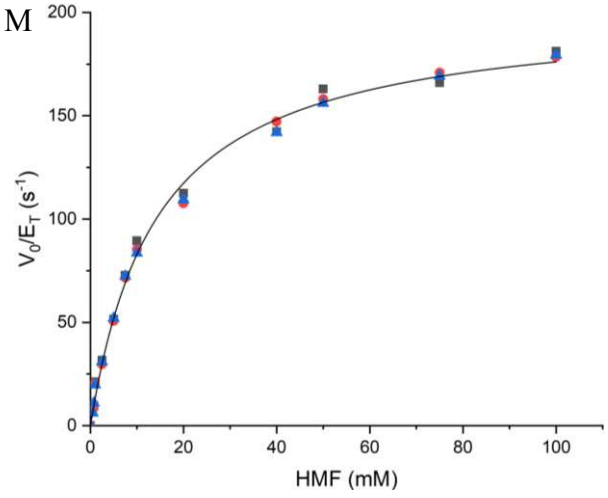
V_0/E_T (s^{-1})
HMF (mM)

N".

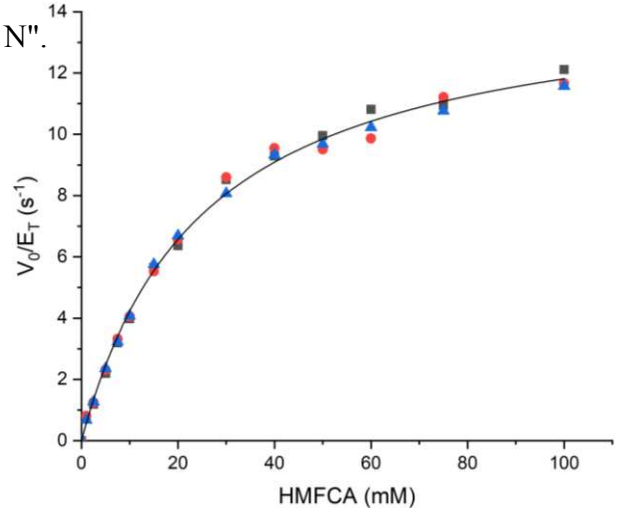
V_0/E_T (s^{-1})
HMFCA (mM)

Figure S5. Initial-rate kinetics. Initial-rate values were measured in triplicate at each substrate concentration. Individual k_{cat} and K_m values were derived by non-linear fitting of the standard Michaelis-Menten or substrate-inhibition (veratryl alcohol) equations to the data using OriginLab 9.55. For substrates that did not display saturation kinetics, composite k_{cat}/K_m values were calculated from the slope of linear fits. Individual substrates are indicated in the x-axis labels of Panels A-N for *Cgr*AAO-WT; A'-N' for *Cgr*AAO-Y334W and A"-N" for *Cgr*AAO-Y334F**.**

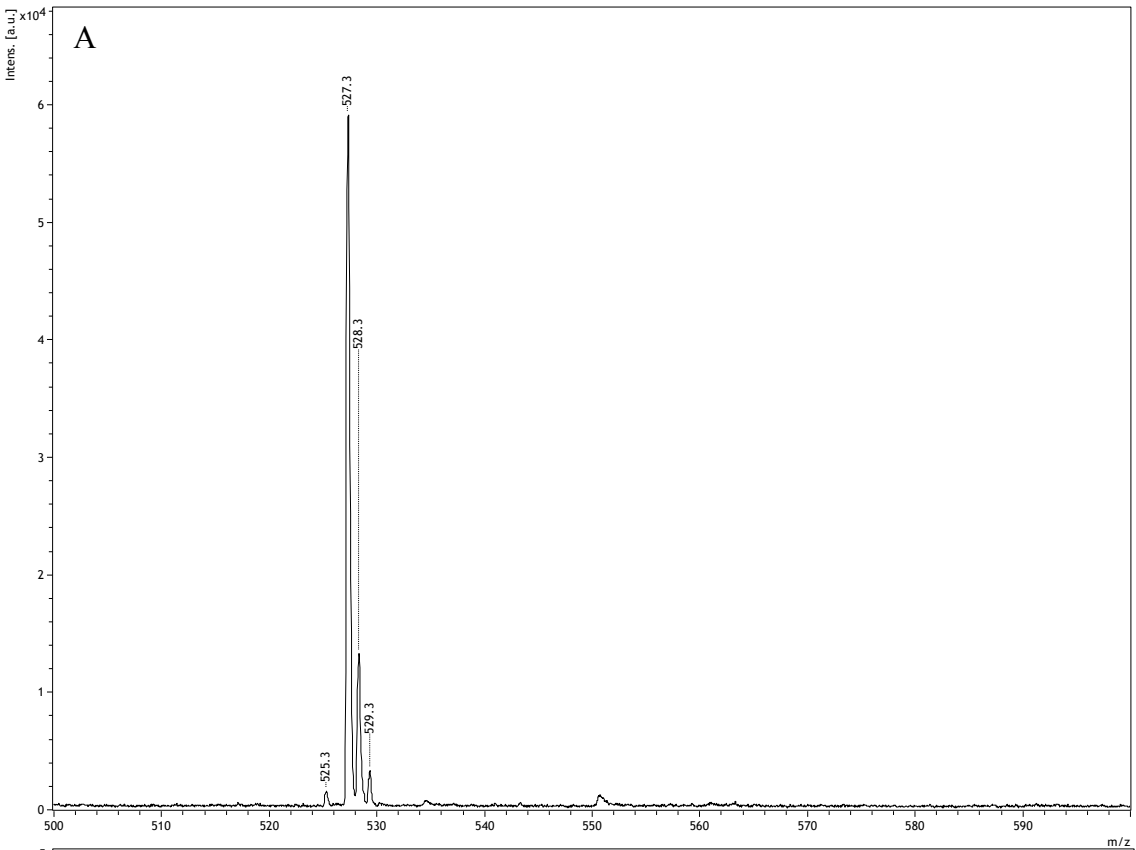
A
Intens. [a.u.]
x10^4
527.3
528.3
529.3
525.3
m/z

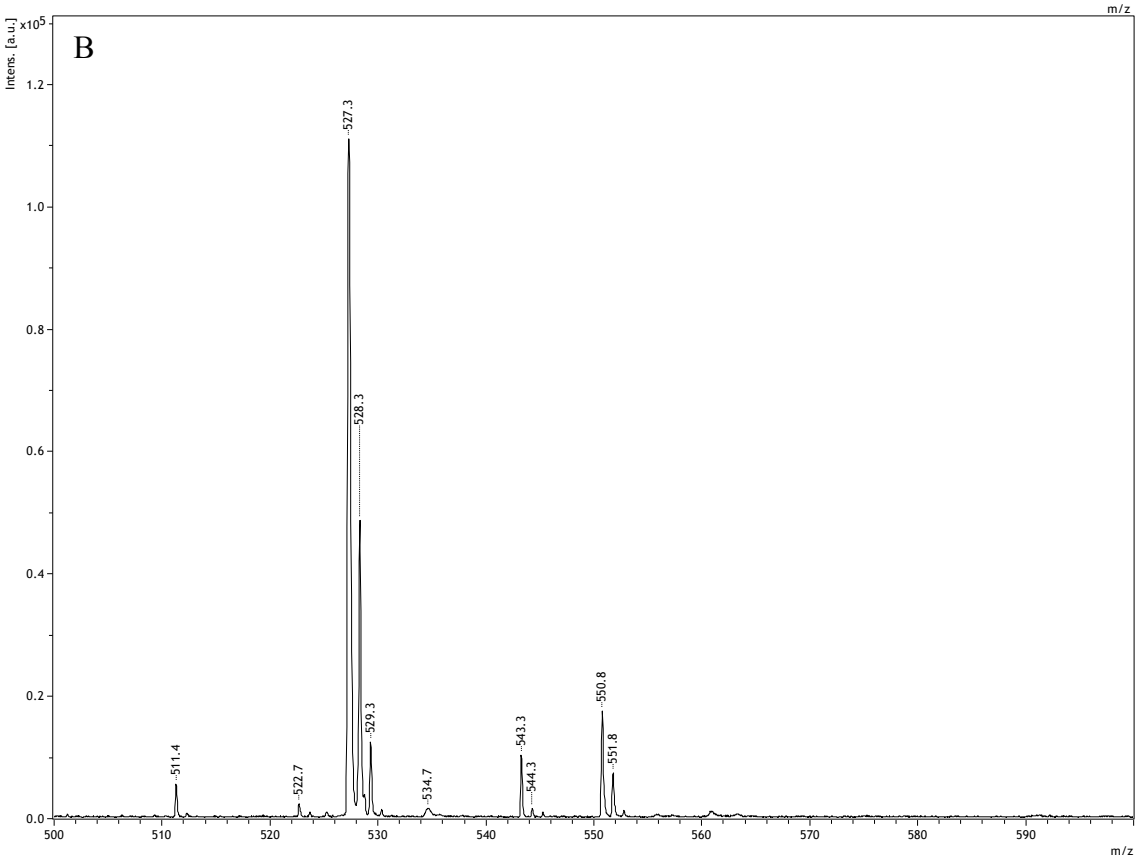
B
Intens. [a.u.]
x10^5
527.3
528.3
529.3
511.4
522.7
534.7
543.3
544.3
550.8
551.8
m/z

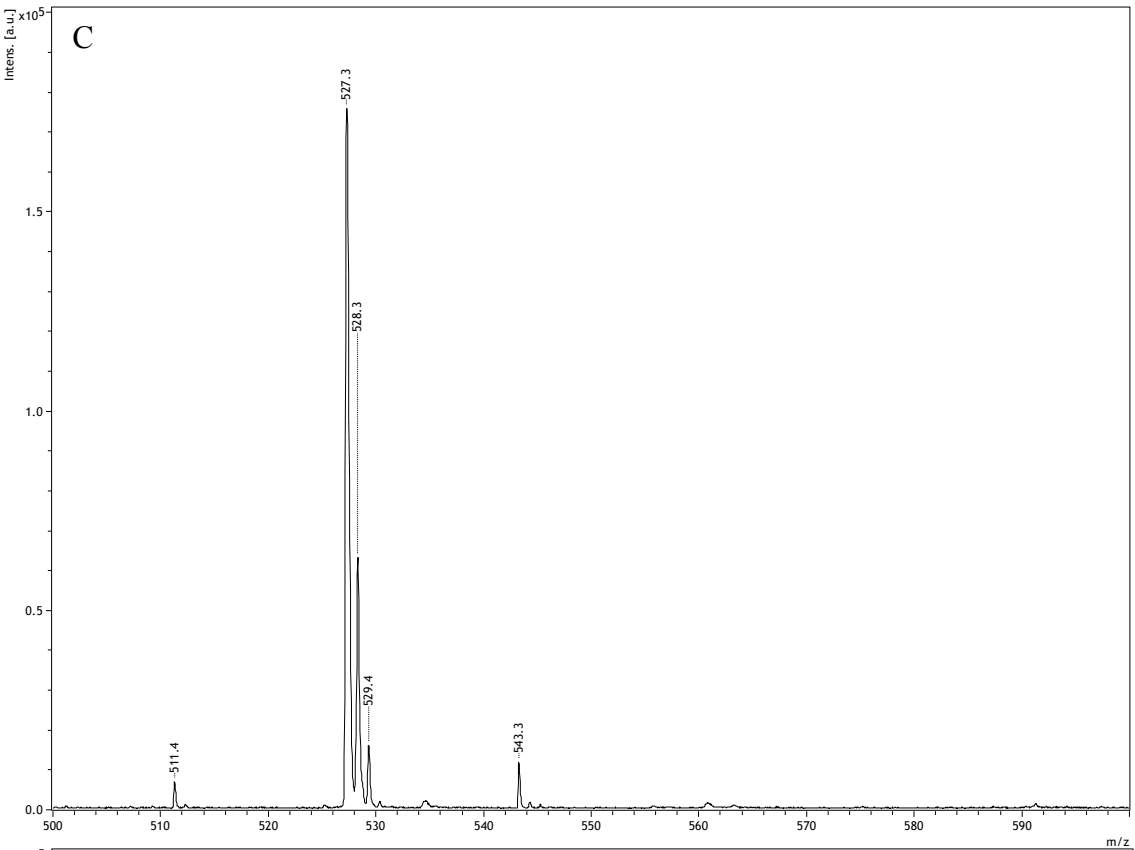
C
Intens. [a.u.]
x10^5
1.5
1.0
0.5
0.0
527.3
528.3
529.4
511.4
543.3
500
510
520
530
540
550
560
570
580
590
m/z

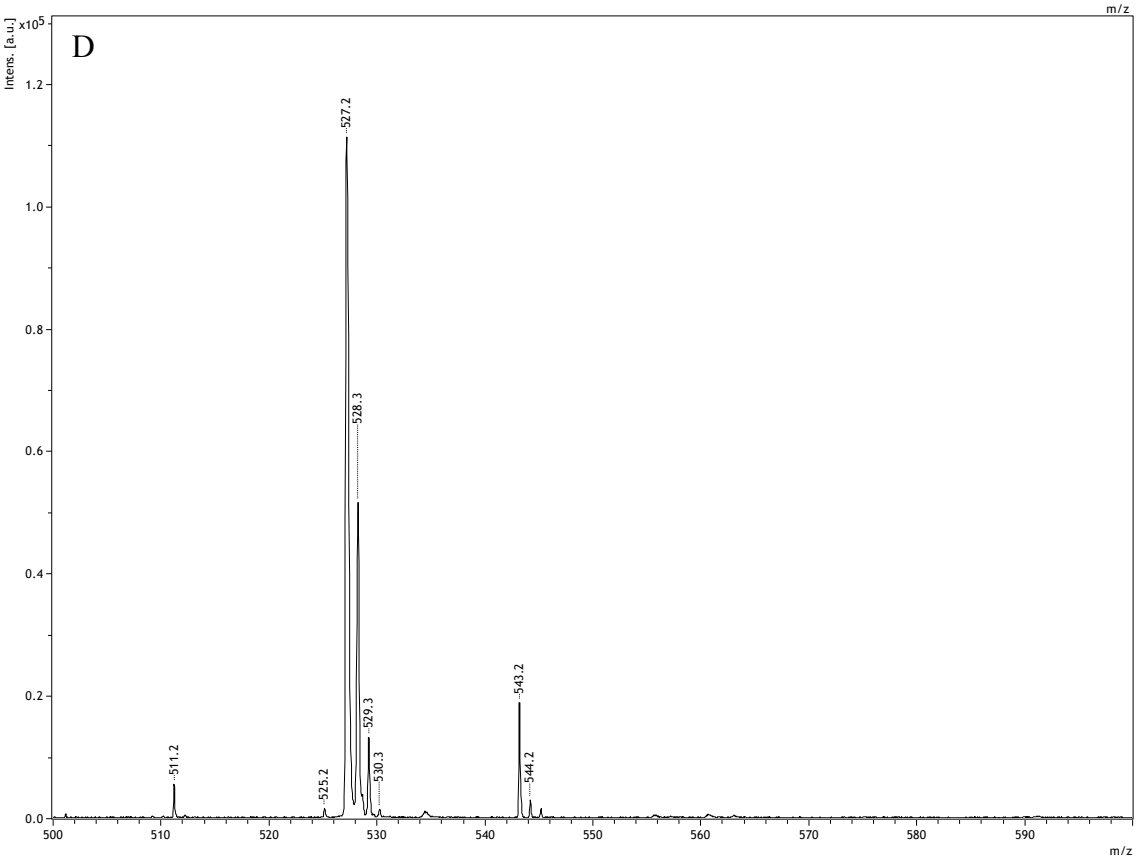
D
Intens. [a.u.]
x10^5
1.2
1.0
0.8
0.6
0.4
0.2
0.0
527.2
528.3
529.3
543.2
511.2
525.2
530.3
544.2
500
510
520
530
540
550
560
570
580
590
m/z

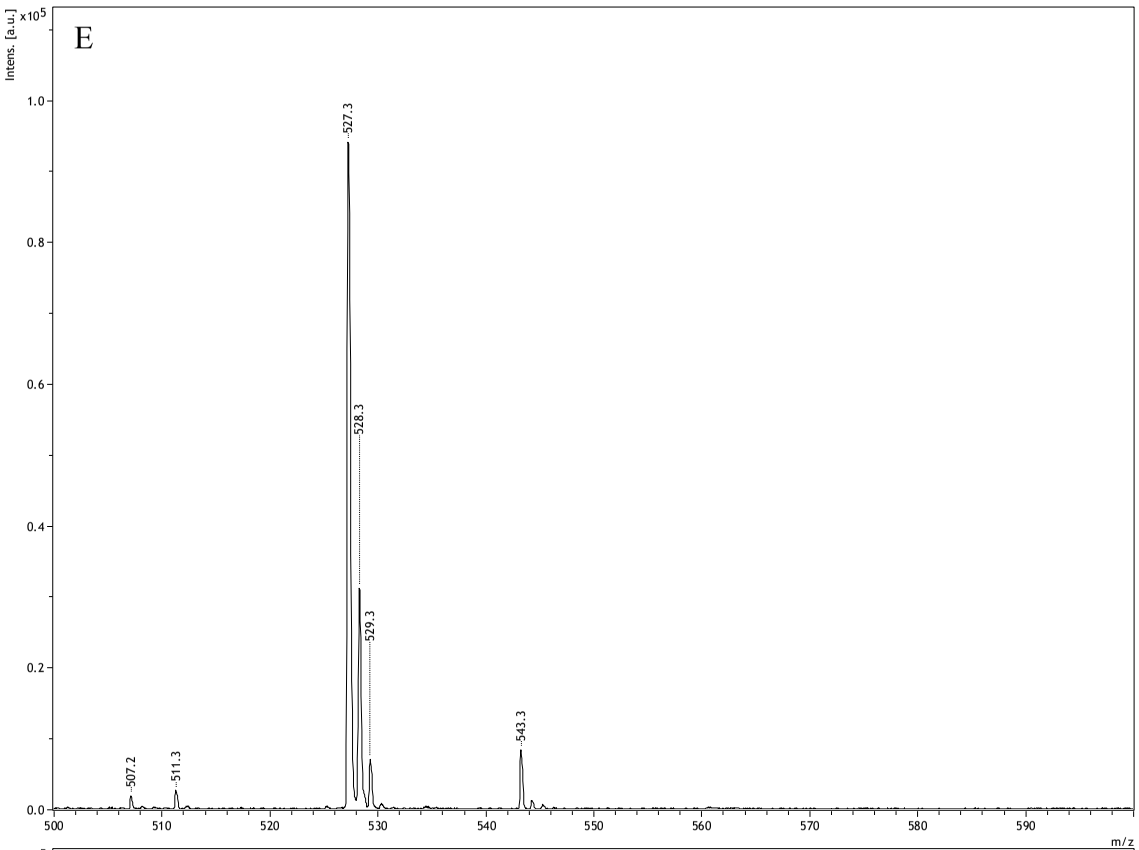
E
Intens. [a.u.]
x10^5
1.0
0.8
0.6
0.4
0.2
0.0
527.3
528.3
529.3
543.3
507.2
511.3
500
510
520
530
540
550
560
570
580
590
m/z

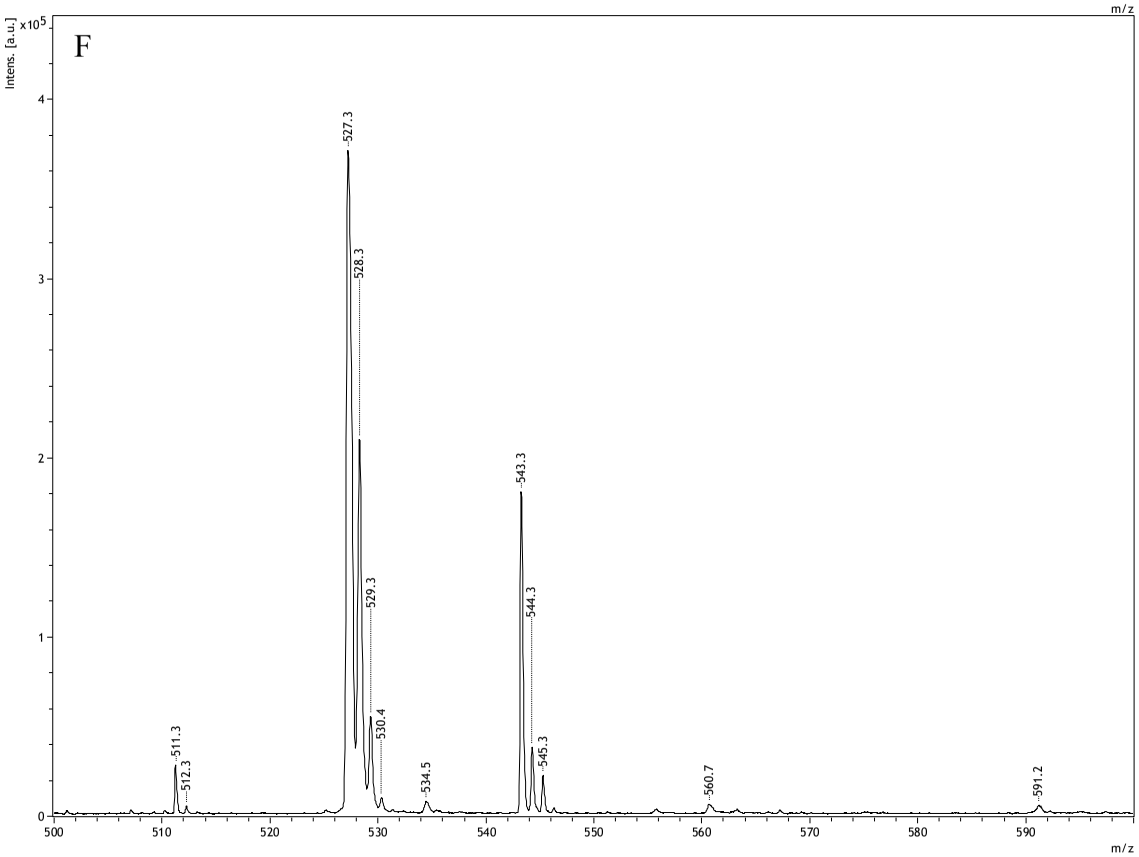
F
Intens. [a.u.]
x10^5
4
3
2
1
0
527.3
528.3
543.3
529.3
544.3
511.3
512.3
530.4
534.5
545.3
560.7
591.2
500
510
520
530
540
550
560
570
580
590
m/z

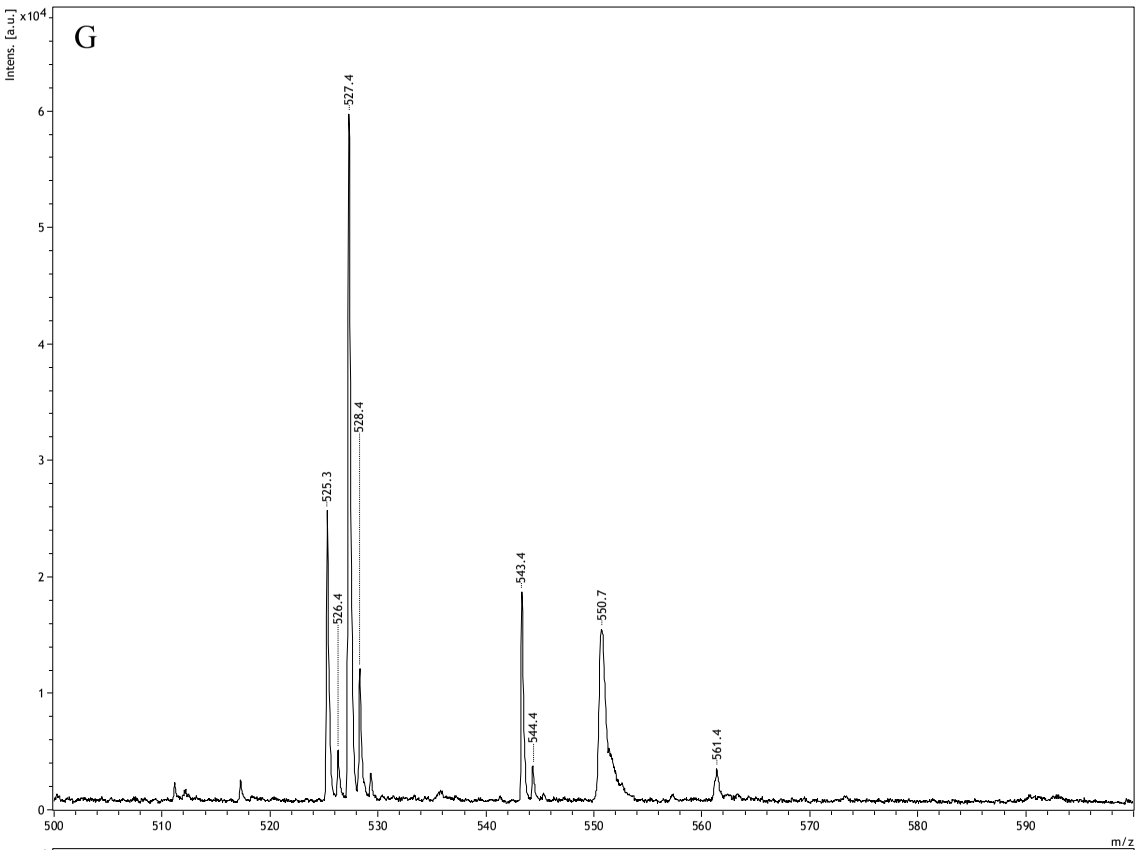
G
Intens. [a.u.]
x10^4
527.4
528.4
525.3
526.4
543.4
550.7
544.4
561.4
m/z

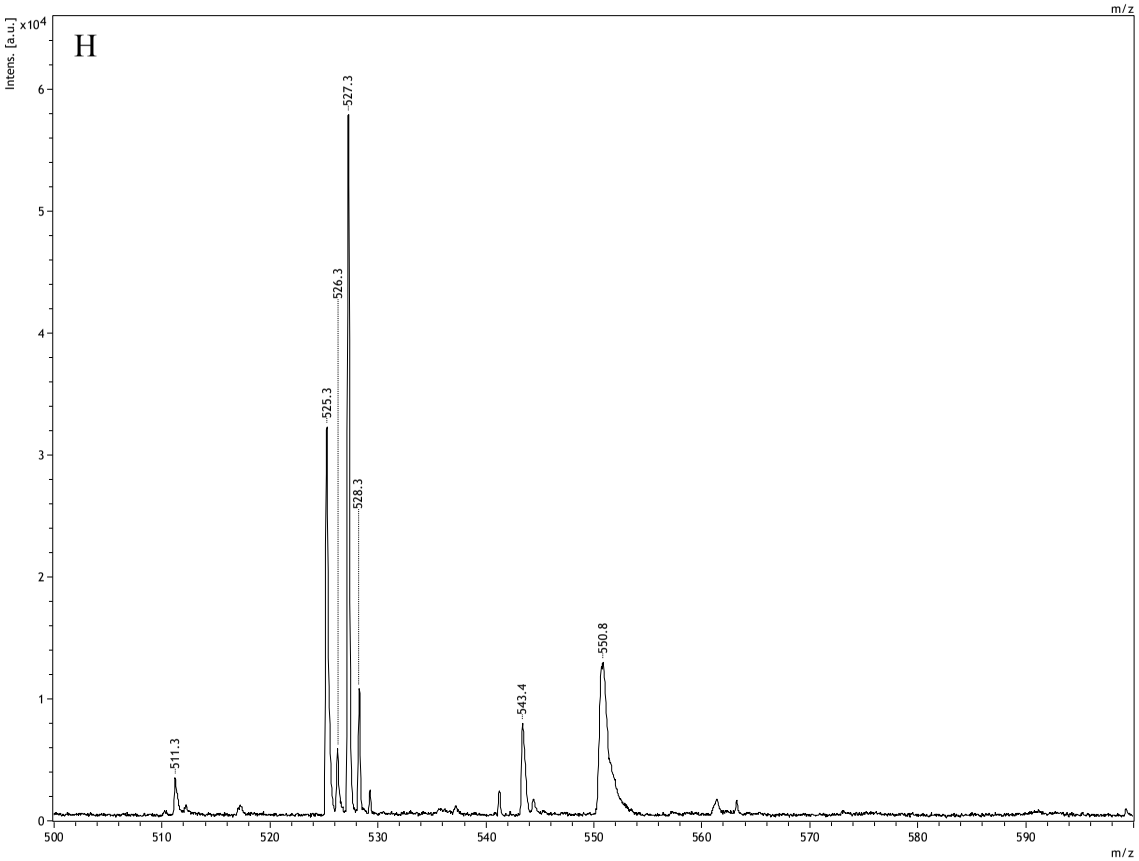
H
Intens. [a.u.]
x10^4
527.3
526.3
525.3
528.3
550.8
543.4
511.3
m/z

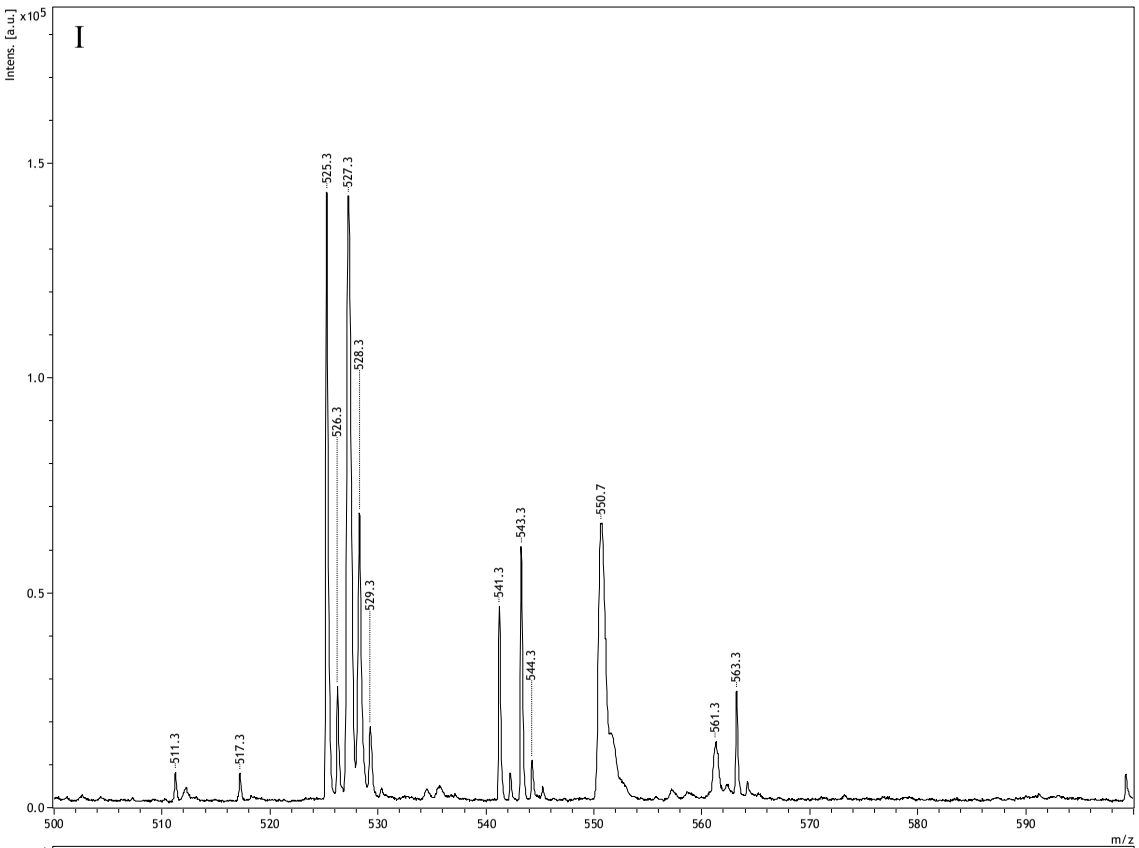
I
Intens. [a.u.]
x10^5
1.5
1.0
0.5
0.0
525.3
527.3
528.3
526.3
529.3
541.3
543.3
544.3
550.7
511.3
517.3
561.3
563.3
500
510
520
530
540
550
560
570
580
590
m/z

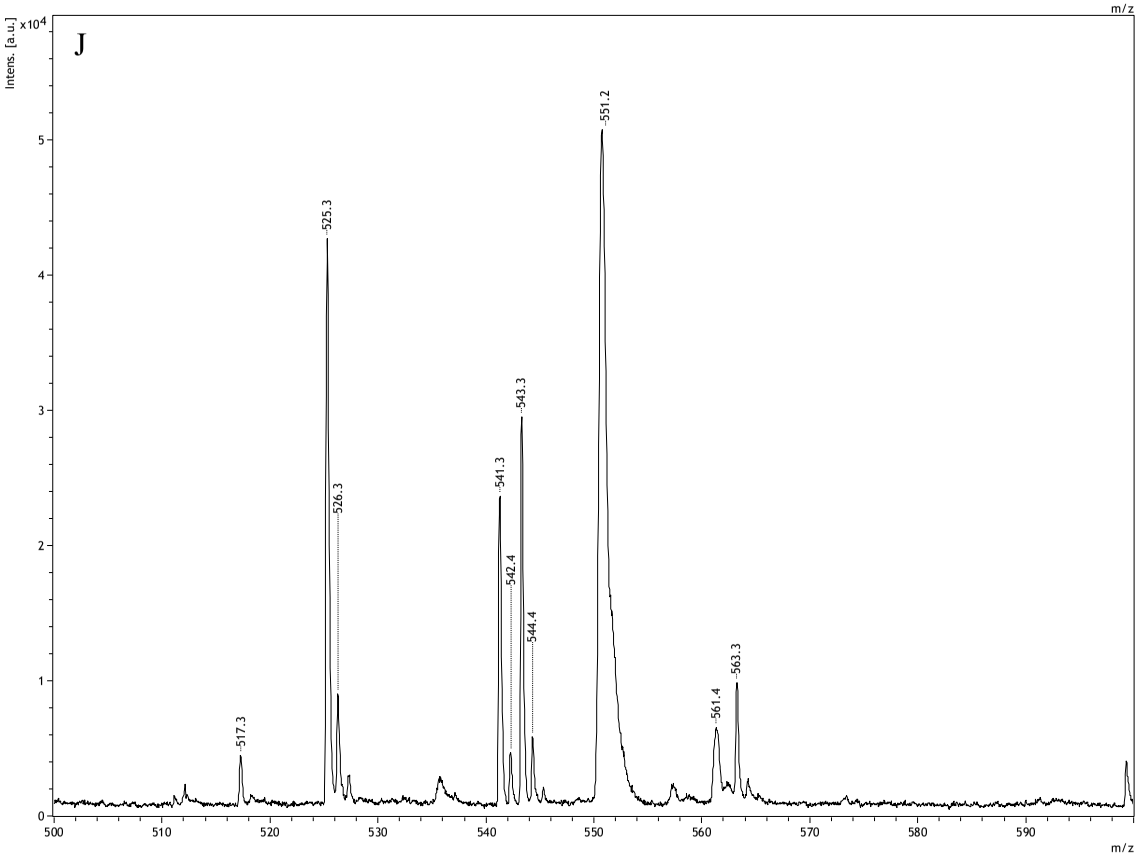
J
Intens. [a.u.]
x10^4
5
4
3
2
1
0
551.2
525.3
543.3
526.3
541.3
542.4
544.4
563.3
517.3
561.4
500
510
520
530
540
550
560
570
580
590
m/z

Figure S6. Time course analysis of raffinose oxidation by *Cgr*AAO by MALDI-TOF. (A-E) 10 mM raffinose incubated with 1 U of HRP/mg of substrate and 115 U of catalase/mg substrate at times 0 h (A), 2 h (B), 4 h (C), 8 h (D) and 16 h (E). (F-J) 10 mM raffinose incubated with 1 U of HRP/mg of substrate, 115 U of catalase/mg substrate and 200 µg of *Cgr*AAO at times 0 h (F), 2 h (G), 4 h (H), 8 h (I) and 16 h (J). m/z 527.3 = raffinose sodium adduct, m/z 525.3 = raffinose aldehyde product sodium adduct, m/z = 543.3 raffinose aldehyde product in hydrate form sodium adduct, m/z = 541.3 uronic acid derivative sodium adduct. The identity of the broad peak at m/z = 550.7 is unknown.

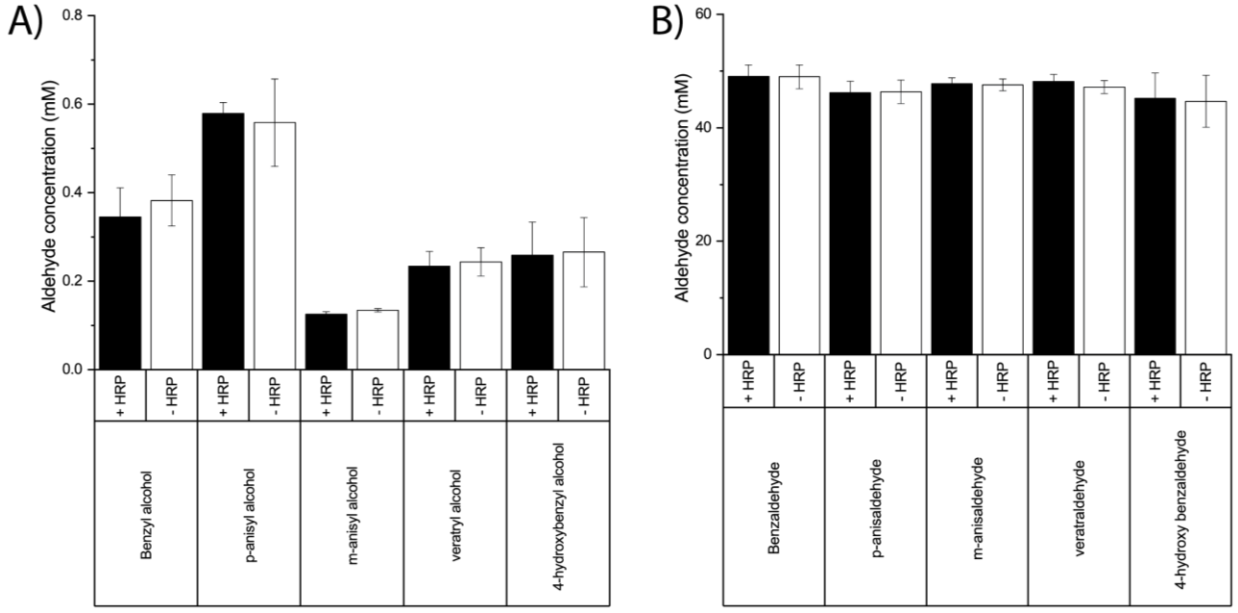

Figure S7. Aldehyde detection by Purpald. (A) 50 mM aryl alcohol incubated with 10 mM H_2O_2 in presence or absence of 2.3 μM HRP for 15 minutes. (B) 50 mM aryl aldehyde incubated with 10 mM H_2O_2 in presence or absence of 2.3 μM HRP for 15 minutes. Standard curves for each aromatic aldehyde made between 20 mM and 100 μM gave a linear response ($r^2 > 0.99$) with a limit of detection of 50 μM.

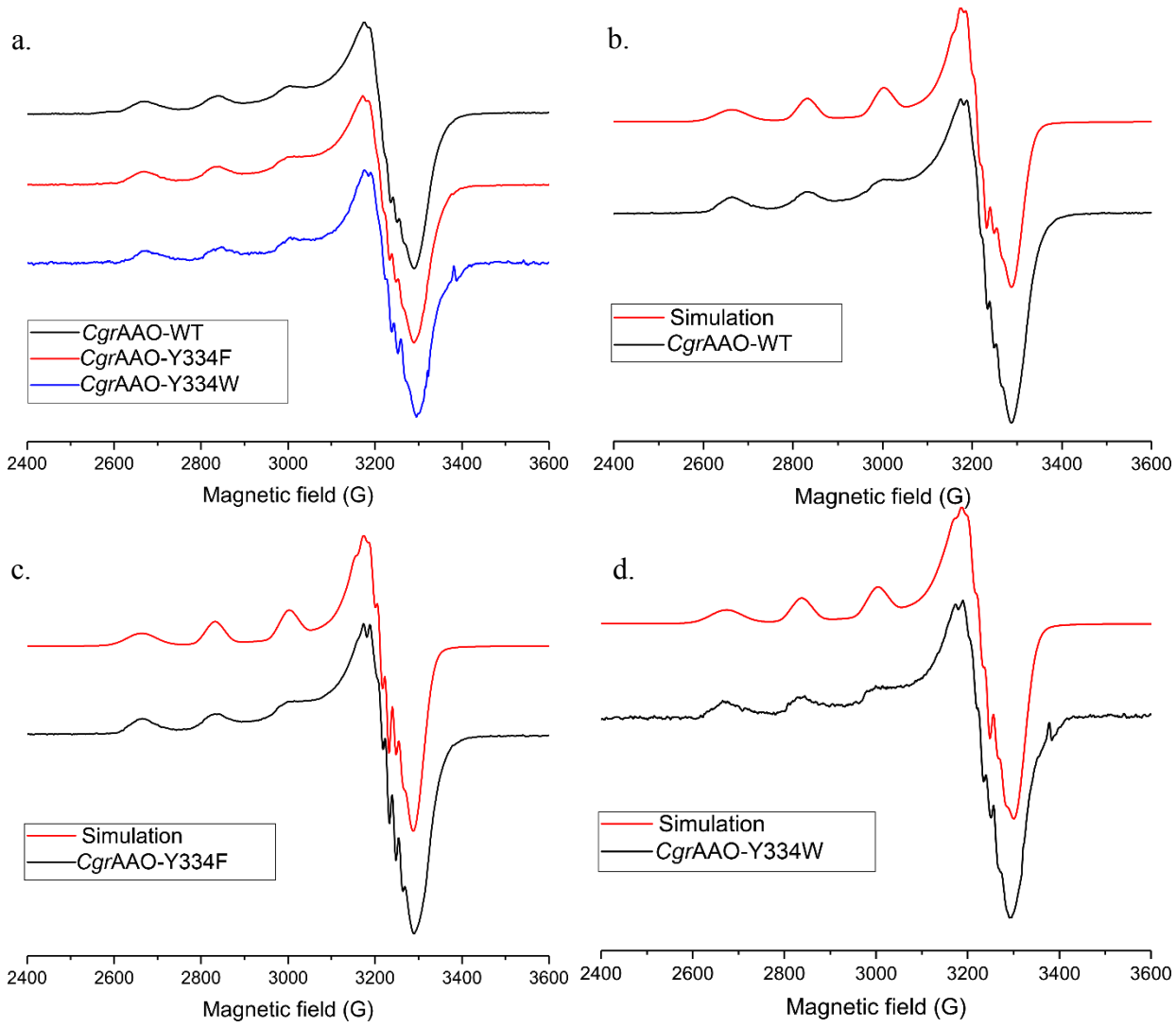

Figure S8: Continuous wave X band frozen solution spectra of *Cgr*AAO$_{(AA5_2)}$-WT, -Y334F and –Y334W collected in 100 mM Na phosphate buffer pH 7.0 without (a) and with 10% (*v/v*) glycerol (b, c, d). Simulations of the experimental data for *Cgr*AAO-WT (b), *Cgr*AAO-Y334F (c) and *Cgr*AAO-Y334W (**d**) are shown in red.

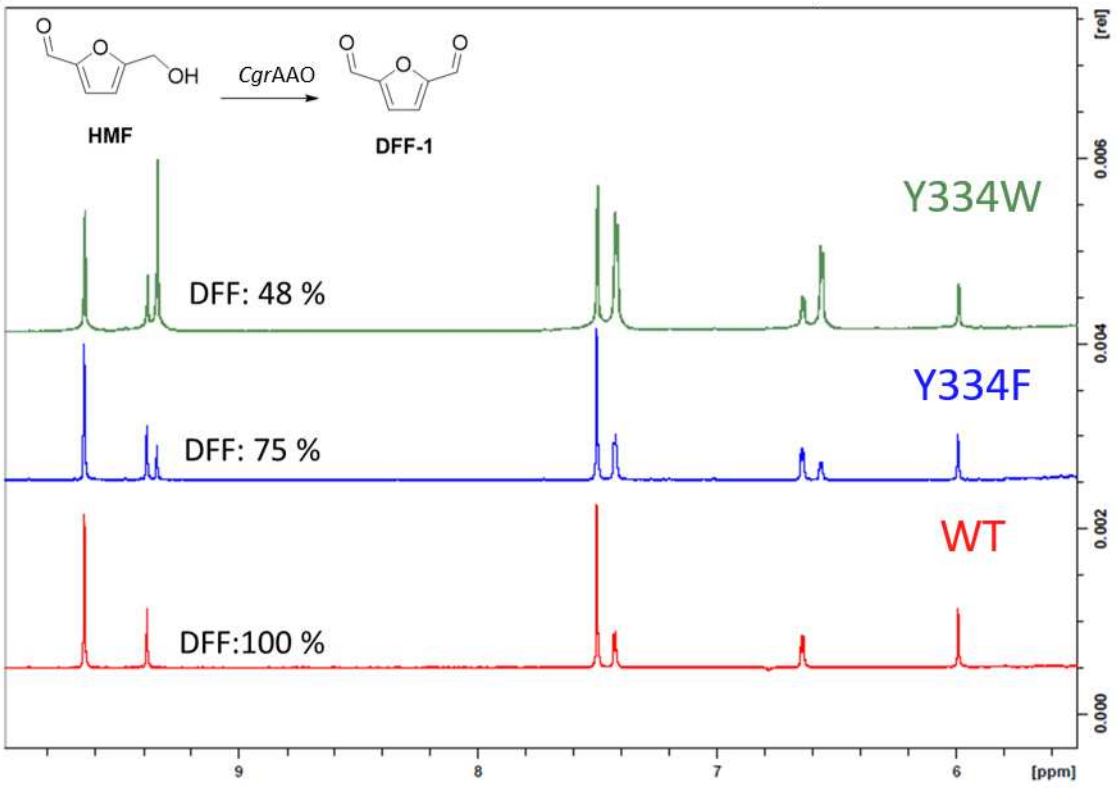

Figure S9. ^{1}H NMR spectra (400 MHz, 1:9 D_2O:phosphate buffer, 20 mM, pH 7) showing product profiles for the oxidation of 20 mM HMF by *Cgr*AAO wild type and variants, as indicated.

Supporting References

1. Dijkman, W. P.; Fraaije, M. W., Discovery and Characterization of a 5-Hydroxymethylfurfural Oxidase from Methylovorus sp. Strain MP688. *Appl. Environ. Microbiol.* **2014,** *80*, 1082-1090.

2. Carro, J.; Ferreira, P.; Rodríguez, L.; Prieto, A.; Serrano, A.; Balcells, B.; Ardá, A.; Jiménez- Barbero, J.; Gutiérrez, A.; Ullrich, R., 5- Hydroxymethylfurfural Conversion by Fungal Aryl- Alcohol Oxidase and Unspecific Peroxygenase. *FEBS J.* **2015,** *282*, 3218-3229.

3. Kadowaki, M.; Godoy, M.; Kumagai, P.; Costa-Filho, A.; Mort, A.; Prade, R.; Polikarpov, I., Characterization of a New Glyoxal Oxidase from the Thermophilic Fungus Myceliophthora thermophila M77: Hydrogen Peroxide Production Retained in 5-Hydroxymethylfurfural Oxidation. *Catalysts* **2018,** *8*, 476.

4. Daou, M.; Yassine, B.; Wikee, S.; Record, E.; Duprat, F.; Bertrand, E.; Faulds, C. B., Pycnoporus cinnabarinus Glyoxal Oxidases Display Differential Catalytic Efficiencies on 5-Hydroxymethylfurfural and its Oxidized Derivatives. *Fungal Biol. Biotechnol.* **2019,** *6*, 4.

5. Abbott, D. W.; Eirín-López, J. M.; Boraston, A. B., Insight into Ligand Diversity and Novel Biological Roles for Family 32 Carbohydrate-Binding Modules. *Mol. Biol. Evol.* **2007,** *25*, 155-167.

6. Tordai, H.; Bányai, L.; Patthy, L., The PAN Module: the N- Terminal Domains of Plasminogen and Hepatocyte Growth Factor are Homologous with the Apple Domains of the

Prekallikrein Family and with a Novel Domain Found in Numerous Nematode Proteins. *FEBS Lett.* **1999,** *461*, 63-67.

7. Oide, S.; Tanaka, Y.; Watanabe, A.; Inui, M., Carbohydrate-Binding Property of a Cell Wall Integrity and Stress Response Component (WSC) Domain of an Alcohol Oxidase from the Rice Blast Pathogen Pyricularia oryzae. *Enzyme Microb. Technol.* **2019,** *125*, 13-20.